Redox Biology 45 (2021) 102057

Contents lists available at ScienceDirect

Redox Biology

journal homepage: www.elsevier.com/locate/redox

Combined glyoxalase 1 dysfunction and vitamin B6 deficiency in a schizophrenia model system causes mitochondrial dysfunction in the prefrontal cortex

Kazuya Toriumi [a,b], Stefano Berto [b,c], Shin Koike [d], Noriyoshi Usui [b,e,f,g], Takashi Dan [h], Kazuhiro Suzuki [a,i], Mitsuhiro Miyashita [a], Yasue Horiuchi [a], Akane Yoshikawa [a,j], Mai Asakura [a], Kenichiro Nagahama [k], Hsiao-Chun Lin [k], Yuki Sugaya [k], Takaki Watanabe [k], Masanobu Kano [k], Yuki Ogasawara [d], Toshio Miyata [h], Masanari Itokawa [a], Genevieve Konopka [b], Makoto Arai [a,*]

[a] Schizophrenia Research Project, Department of Psychiatry and Behavioral Sciences, Tokyo Metropolitan Institute of Medical Science, Tokyo, 156-8506, Japan
[b] Department of Neuroscience, University of Texas Southwestern Medical Center, Dallas, TX 75390-9111, USA
[c] Department of Neuroscience, Medical University of South Carolina, Charleston, SC 29403, USA
[d] Department of Analytical Biochemistry, Meiji Pharmaceutical University, Tokyo 204-8588, Japan
[e] Center for Medical Research and Education, Graduate School of Medicine, Osaka University, Osaka, 565-0871, Japan
[f] Department of Neuroscience and Cell Biology, Graduate School of Medicine, Osaka University, Osaka, 565-0871, Japan
[g] Global Center for Medical Engineering and Informatics, Osaka University, Osaka, 565-0871, Japan
[h] Division of Molecular Medicine and Therapy, Tohoku University Graduate School of Medicine, Sendai, 980-8575, Japan
[i] Department of Psychiatry, Graduate School of Medicine, Shinshu University, Nagano, 390-8621, Japan
[j] Department of Psychiatry and Behavioral Science, Graduate School of Medicine, Juntendo University, Tokyo, 113-8421, Japan
[k] Department of Neurophysiology, Graduate School of Medicine, The University of Tokyo, Tokyo 113-0033, Japan

ARTICLE INFO

Keywords:
Glyoxalase 1
Vitamin B6
Methylglyoxal
Schizophrenia
Mitochondria
Oxidative stress

ABSTRACT

Methylglyoxal (MG) is a reactive and cytotoxic α-dicarbonyl byproduct of glycolysis. Our bodies have several biodefense systems to detoxify MG, including an enzymatic system by glyoxalase (GLO) 1 and GLO2. We identified a subtype of schizophrenia patients with novel mutations in the *GLO1* gene that results in reductions of enzymatic activity. Moreover, we found that vitamin B6 (VB6) levels in peripheral blood of the schizophrenia patients with *GLO1* dysfunction are significantly lower than that of healthy controls. However, the effects of *GLO1* dysfunction and VB6 deficiency on the pathophysiology of schizophrenia remains poorly understood. Here, we generated a novel mouse model for this subgroup of schizophrenia patients by feeding *Glo1* knockout mice VB6-deficent diets (KO/VB6(−)) and evaluated the combined effects of *GLO1* dysfunction and VB6 deficiency on brain function. KO/VB6(−) mice accumulated homocysteine in plasma and MG in the prefrontal cortex (PFC), hippocampus, and striatum, and displayed behavioral deficits, such as impairments of social interaction and cognitive memory and a sensorimotor deficit in the prepulse inhibition test. Furthermore, we found aberrant gene expression related to mitochondria function in the PFC of the KO/VB6(−) mice by RNA-sequencing and weighted gene co-expression network analysis (WGCNA). Finally, we demonstrated abnormal mitochondrial respiratory function and subsequently enhanced oxidative stress in the PFC of KO/VB6(−) mice in the PFC. These findings suggest that the combination of *GLO1* dysfunction and VB6 deficiency may cause the observed behavioral deficits via mitochondrial dysfunction and oxidative stress in the PFC.

1. Introduction

Methylglyoxal (MG) is a highly reactive α-ketoaldehyde formed endogenously as a byproduct of the glycolytic pathway, by the degradation of triphosphates or by nonenzymatic fragmentation of sugar [1]. MG accumulates under conditions of hyperglycemia, impaired glucose

* Corresponding author. Schizophrenia Research Project, Department of Psychiatry and Behavioral Sciences, Tokyo Metropolitan Institute of Medical Science, 2-1-6 Kamikitazawa, Setagaya-ku, Tokyo, 156-8506, Japan.
E-mail address: arai-mk@igakuken.or.jp (M. Arai).

https://doi.org/10.1016/j.redox.2021.102057
Received 28 May 2021; Received in revised form 21 June 2021; Accepted 22 June 2021
Available online 24 June 2021

metabolism, or oxidative stress. An excess of MG formation causes mitochondrial impairment and reactive oxygen species (ROS) production that further increases oxidative stress. It also leads to the formation of advanced glycation end products (AGEs) due to MG reacting with proteins, DNA, and other biomolecules [2,3], which can induce aberrant inflammation via binding to receptors for AGEs (RAGE) [4,5]. These effects imply that accumulating MG causes damage in a number of tissues and organs [6], resulting in aging and diabetic complications, such as neuropathy, retinopathy, and ischemic heart disease. *In vivo,* a glyoxalase system works to remove the toxic MG. The glyoxalase system comprised of two enzymes, glyoxalase (GLO) 1 and GLO2 is an enzymatic pathway that catalyzes the glutathione-dependent detoxification of MG. GLO1 and GLO2 are ubiquitously expressed in various tissues—including the brain—and provide an effective defense against the accumulations of MG.

Schizophrenia is a heterogeneous psychiatric disorder characterized by positive symptoms, such as hallucinations and delusions, negative symptoms, such as anhedonia and flat affect, and cognitive impairment. We have reported that *GLO1* activity in patients with schizophrenia is significantly lower than healthy controls, and we identified several schizophrenia patients with a novel heterozygous frameshift and a single nucleotide variation (SNV) in *GLO1* gene that results in reductions of enzymatic activity [7]. Furthermore, we found that vitamin B6 (VB6) levels in peripheral blood of the schizophrenia patients with *GLO1* dysfunction are significantly lower than that of healthy controls [7]. More than 35% of patients with schizophrenia have low levels of VB6 (clinically defined as male: < 6 ng/ml, female: < 4 ng/ml). Other groups have replicated these results [8,9]. VB6 levels are inversely proportional to the severity score on the Positive and Negative Syndrome Scale (PANSS) [10]. Also, a recent review has shown the decreased VB6 in patients with schizophrenia as the most convincing evidence in peripheral biomarkers for major mental disorders [11]. Moreover, we recently reported that high-dose VB6 treatment was effective in alleviating psychotic symptoms (especially PANSS negative and general subscales), in a subset of patients with schizophrenia, coincident with decreased AGEs levels in the peripheral blood [12]. Despite this evidence, the effects of *GLO1* dysfunction and VB6 deficiency on the pathophysiology of schizophrenia *in vivo* remain unclear.

In the present study, we generated *Glo1* KO mice to uncover the influence of GLO1 dysfunction on behavioral performances and neurochemical function. We found that *Glo1* KO mice fed with VB6-lacking (VB6(−)) diets exhibited an accumulation of homocysteine in plasma and MG within the brain and behavioral deficits including sensorimotor deficit in a prepulse inhibition (PPI) test, although the *Glo1* gene deletion or VB6 deficiency alone did not cause the characteristic changes. Furthermore, we found aberrant gene expression involved in mitochondria function in the prefrontal cortex (PFC) of the *Glo1* KO mice with VB6 deficiency and we demonstrated respiratory impairment in mitochondria and enhanced oxidative stress within the PFC of *Glo1* KO mice with VB6 deficiency.

2. Material and methods

2.1. Generation of Glo1 knockout mice

A 129/Sv-derived ES cell line (S17–2B1) containing a gene trap cassette in the *Glo1* gene locus was purchased from Mutant Mouse Regional Resource Centers (http://www.mmrrc.org/). The ES cells were microinjected into embryonic day 3.5 (E3.5) blastocysts (genotype C57BL/6J) and then transferred into pseudopregnant ICR females for the generation of chimeras. Chimerism of newborn mice was assessed by coat color inspection. A male chimera with high ES cell contribution (100% agouti coat color) was crossed with C57BL/6J mice. The germline transmission was judged by the presence of agouti pups (F1 generation) and disrupted alleles identified by PCR genotyping as indicated below.

One pair of heterozygous (HE) F1 mice were mated to confirm whether the generated F2 *Glo1* KO mouse was nonlethal and normal judging by appearances or not. One randomly selected HE F1 male mouse was backcrossed onto C57BL/6J female mice. The procedure was repeated for ten generations. The HE F11 mice were intercrossed and the behavioral tests were performed with the F12 generation. KO, HE, and wild-type mice (WT) were identified by PCR genotyping before use.

2.2. Glo1 mRNA expression analysis

Total RNAs were extracted from the brains of KO, HE or WT mice using the Fast Pure RNA kit (Takara). The purified RNA samples were used as templates for reverse transcription reactions. Qualitative PCR assays for wild-type transcripts of *Glo1* or fusion transcripts of *Glo1* exon 1 and βGEO were performed. Quantitative PCR for *Glo1* was performed with iQ SYBR Green Supermix and amplified PCR products were measured by the iCycler iQ real-time PCR analyzing system (Bio-Rad).

2.3. GLO1 activity assay

GLO1 enzymatic activity was determined using the spectrophotometric method as described previously with minor modifications [13]. Whole brains were homogenized in a complete Lysis-M reagent (Sigma-Aldrich) containing a protease inhibitor cocktail (cOmplete: Sigma-Aldrich) and a phosphatase inhibitor (PhosSTOP: Sigma-Aldrich). After centrifugation at 15,000 rpm for 15 min at 4 °C, the supernatants were collected and diluted to 1 mg/ml in the Lysis-M reagent. The substrate of *GLO1*, hemithioacetal, was prepared by preincubation of 2 mM methylglyoxal with 2 mM glutathione in a 50 mM sodium phosphate buffer (pH 6.6) at 37 °C for 10 min. The supernatants of the brain (4 μl) were mixed with the hemithioacetal solution (196 μl), and displayed an absorbance at 240 nm, owing to the formation of S-D-lactoylglutathione as measured for 15 min by a microplate spectrophotometer EPOCH2 (BioTek).

2.4. Forced swimming test

Each mouse was placed in an opaque polyvinyl bucket (24 cm high, 23 cm in diameter), which contained water at 22–23 °C to a depth of 15 cm, and was forced to swim for 10 min. The duration of swimming was measured using an infrared detector (Muromachi Kikai Co. Ltd., Japan). The duration of swimming was measured every minute by an infrared detector. Immobility time was calculated as follows: total time (sec) – swimming time (sec) = immobility time (sec).

2.5. Prepulse inhibition (PPI) test

PPI of the acoustic startle response was measured using an SR-LAB System (San Diego Instruments). The stimulus consisted of a 20-ms prepulse, a 100-ms delay, and then a 40-ms startle pulse. The intensity of the prepulse was 4, 8, or 16-dB above the 70-dB background noise. The amount of PPI was calculated as a percentage of the 120-dB acoustic startle response: 100 – [(startle reactivity on prepulse + startle pulse)/ startle reactivity on startle pulse] x 100.

2.6. Locomotor activity test

Locomotor activity was measured using an infrared detector (Muromachi Kikai Co. Ltd., Japan). Mice were placed in a plastic round arena (27 cm high, 27 cm in diameter) and locomotor activity was measured over a period of 2 h.

2.7. Novel object recognition test

The novel object recognition test was performed as described previously with minor modifications [14]. The test procedure consisted of

three sessions: habituation, training, and retention. Each mouse was individually habituated to the box, with 10 min of exploration in the absence of objects each day for 3 consecutive days (Day 1–3) (habituation session). On day 4, each animal was allowed to explore the box for 10 min, in which two novel objects were placed symmetrically. The time spent exploring each object was recorded (training session). The objects were different in shape and color but similar in size. Mice were considered to be exploring an object when their heads were facing it or when they were sniffing it at a distance of less than 2 cm and/or touching it with their nose. After the training session, mice were immediately returned to their home cages. On day 5, the animals were placed back into the same box with one of the familiar objects used in the training session and one novel object. Mice were allowed to explore freely for 5 min and the time spent exploring each object was recorded (retention session). An exploratory preference, the ratio of time spent exploring either of the two objects (training session) or the novel object (retention session) over the total amount of time spent exploring both objects, was used to assess recognition memory.

2.8. Social interaction test

Twelve-week-old male mice were tested for social behavior using the three-chamber social approach paradigm. The apparatus was a square field (W50 × D50 × H40 cm) that is divided into three chambers of equal size by grey walls, which was placed in a dark, sound-attenuated room. During a habituation session, two empty wire cages were placed in the lateral chambers. The mice were placed in the center chamber and allowed to freely explore all chambers for 10 min. Immediately after the habituation session, the mouse was placed in a home cage for 3 min. After the interval, a test session started. The mice were placed in the center chamber again and allowed to freely explore the left and right arenas, which contained a social target (unfamiliar C57BL/6J male mouse) in one chamber and empty in the other chamber. Experimental mice were given 10 min to explore both chambers. The amount of time spent in the lateral chambers and the quadrant around each wire cage as interaction time (that is, sniffing, approach) was recorded and analyzed by the EthoVision tracking system (Noldus, Netherland).

2.9. Induction of VB6 deficiency

To induce VB6 deficiency, WT and KO mice were fed with a VB6-lacking diet containing 5 μg/100 g VB6 pellets from 8 to 12 weeks of age, while control mice in normal VB6 condition were fed with a normal diet, with 1.4 mg/100 g VB6 pellets. Food and tap water were available *ad libitum*.

2.10. Measurement of VB6 and homocysteine in mouse plasma

VB6 and homocysteine concentration in plasma was determined with ID-Vit VB6 (Immunodiagnostic AG: Bensheim, Germany) and homocysteine ELISA kit (Cell Biolabs Inc., CA), respectively, according to the manufacturer's protocol.

2.11. Measurement of methylglyoxal in the brain

Methylglyoxal in the brain was quantified using high-performance liquid chromatography with fluorescence (HPLC-FL) as described previously [15,16]. Brain tissues were homogenized using BioMasher (Nippi, Japan) with nine volumes of ice-cold buffer: 0.1 M phosphate buffer [pH 7.8] and a protease inhibitor cocktail (Nacalai Tesque, Japan). The brain extracts were centrifuged at 12,000×*g* for 10 min at 4 °C. Subsequently, trichloroacetic acid was added to a final concentration of 4% and centrifuged at 12,000×*g* for 10 min at 4 °C. The supernatant was diluted with an equal volume of 1,2-diamino-4, 5-methylenedioxybenzene (MDB) solution and incubated at 60 °C for 40 min in the dark. This MDB-derived sample was then analyzed using HPLC-FL. Ten microliters of the resulting mixture were injected into a C18 column pre-equilibrated with a mobile phase solution, which consisted of water, methanol, and acetonitrile in the ratio 10:7:3. A flow rate of 1.0 ml/min was used with a running time of 7 min. The retention times and peak areas were monitored at excitation and emission wavelength of 355 nm and 393 nm, respectively.

2.12. RNA sequencing

RNA-sequencing (RNA-seq) was performed as described previously [17]. Briefly, total RNA from the PFC, STR, and HIP was extracted with the miRNeasy Mini Kit (Qiagen, 217004) according to the manufacturer's instructions. RNA integrity number (RIN) of total RNA was quantified by an Agilent 2100 Bioanalyzer using an Agilent RNA 6000 Nano Kit (Agilent, 5067–1511). Total RNAs with an average RIN value of 8.52 ± 0.05 were used for RNA-seq library preparation. mRNA was purified from 2 μg of total RNA by NEXTflex poly(A) beads (Bioo Scientific, 512981), subjected to fragmentation and first and second strand syntheses, and cleaned up by EpiNext beads (EpiGentek, P1063). The second strand DNA was adenylated, ligated, and cleaned up twice by EpiNext beads. cDNA libraries were amplified by PCR and cleaned up twice by EpiNext beads. cDNA library quality was quantified by a 2100 Bioanalyzer using an Agilent high-sensitivity DNA kit (Agilent, 5067–4626). Libraries were sequenced separately as 75-bp single ends on an Illumina NextSeq 500.

2.13. RNA-seq data processing

An in-house RNA-seq pipeline was established for RNA-seq data analysis and processing. Reads were aligned to the mouse mm10 reference genome using STAR 2.5.2b [18] with the following parameter –outFilterMultimapNmax 10 –alignSJoverhangMin 10 –alignSJDBoverhangMin 1 –outFilterMismatchNmax 3 –twopassMode Basic. Gencode annotation for mm10 (version vM11) was used as a reference to build STAR indexes and alignment annotation [19]. For each sample, a BAM file including mapped and unmapped with spanning splice junctions was produced. Secondary alignment and multi-mapped reads where further removed using in-house scripts. Only uniquely mapped reads were retained for further analysis.

Overall quality control metrics were performed using RseqQC using the UCSC mm10 gene model provided [20]. This includes the number of reads after multiple-step filtering, ribosomal RNA reads depletion, reads mapped to an exon, UTRs, and intronic regions.

Gene level expression was calculated using HTseq version 0.6.0 using intersection-strict mode by exonic regions [21]. Counts were calculated based on protein-coding genes annotation from mm10 Gencode gtf file (version vM11). CPM (counts per million reads) was calculated using edgeR [22]. To retain only expressed genes, we used a "by condition" log2(CPM + 1) cutoff. Briefly, a gene is considered expressed with log2 (CPM + 1) ≥ 0.5 in all four replicates of a given condition (WT/VB6(+), WT/VB6(−), KO/VB6(+), KO/VB6(−)). In total, we detected 13428 protein-coding genes expressed in our data. We further used those genes for differential and co-expression analyses.

2.14. Differential expression analysis

Differential expression was assessed using the DESeq2 package in R [23]. We applied the following method on all the pairwise comparisons between WT and KO, with/without VB6 in the diet.

The expression matrix contained the 13428 protein-coding genes that passed the log2(CPM + 1) ≥ 0.5 cut-off in all four replicates of an experimental condition and the covariate matrix including RIN values and Batches were included.

Using the SVA package in R [24], we identified potential unwanted surrogate variables (2 surrogate variables).

Linear regression was performed using DESeq2 to remove covariate

variables:

Gene expression ~ SVA1 + SVA2 + Batch

We calculated differentially expressed genes (DEGs) using criteria of FDR $\leq$ 0.05 and log2(fold change) $\geq$ |0.3|. A permutation test was additionally applied using 1000 permuted experiments. None of the permuted analyses showed the same genes differentially expressed (permutation $p < 0.001$).

Gene ontology (GO) analysis of the significant DEGs was carried out using ToppGene (https://toppgene.cchmc.org), and the resultant GO terms were consolidated using REVIGO (reduce and visualize GO) [25].

2.15. Co-expression network analysis (WGCNA)

To identify the modules of co-expressed genes, we carried out weighted gene co-expression network analysis (WGCNA) [26] on the RNA-seq data. As input, we used log2(CPM+1) values of the 13428 protein-coding expressed genes. Batch effects were further removed using the ComBat function in the SVA package in R [24]. We generated a signed network by using the blockwiseModules function in the WGCNA package. Beta was chosen as 14 so the network has a high scale-free R square ($r^2 = 0.79$). For other parameters, we used corType = bicor, maxBlockSize = 14000, mergingThresh = 0.10, reassignThreshold = 1e-5, deepSplit = 4, detectCutHeight = 0.999, and minModuleSize = 50. Then the modules were determined by using the dynamic tree-cutting algorithm.

The top 250 edges based on ranked weight were plotted to represent the modules showing the top hub genes. We used Cytoscape 3.7.2 for data visualization and optimization [27].

2.16. Identification of cell type preferential expression

To identify cell type preferential expression of the DEGs and detected modules, we used a scRNA-seq data from mouse brain curated from DropViz database [28]. Cell-types markers were downloaded and used for the enrichment test. We used a Fisher's exact test in R with the following parameters: alternative = "greater", conf.level = 0.99. We reported Odds Ratio (OR) and Benjamini-Hochberg adjusted *P*-values (FDR). This method was used for both DEGs and the WGCNA module enrichment described below.

2.17. Collected data sources

Only genes that are expressed in the mouse brain samples are included as the background information. The ASD-related genes were obtained from the Simons Foundation Autism Research Initiative [29]. ASD modules were downloaded from an independent publication [30]. Intellectual disability genes were collected from multiple independent sources [31]. Genes related to synapse were downloaded from the SynaptomeDB [32]. Schizophrenia associated genes were curated from the SZGR database [33]. For fragile X mental retardation (FMRP) gene targets, we used an independent publication [34]. Epilepsy associated genes were curated from the Epilepsy Gene Database [35]. scRNA-seq from mouse brain was curated from DropViz database [28]. Modules associated with neuropsychiatric disorders were curated from an independent publication [36]. All genes from human collections were translated into mouse gene IDs using the biomaRt package in R [37].

2.18. Measurement of respiratory function in isolated PFC mitochondria

Mitochondria were isolated from the PFC with a mitochondria isolation kit for tissue and cultured cells (Biochain Institute, CA) according to the manufacturer's protocol.

Respiratory function in the isolated mitochondria was quantified using extracellular Flux Analyzer Seahorse XFe96 (Agilent technologies) as described previously with minor modifications [38,39]. Isolated mitochondria were diluted at 0.2 mg/ml with mitochondria assay solution [70 mM sucrose, 210 mM mannitol, 2 mM HEPES, 5 mM $MgCl_2$, 10 m M KH_2PO_4, 0.2% fatty acid-free BSA, 10 mM sodium pyruvate, 2 mM D-malic acid (pH 7.4)]. The mitochondria (100 μl) were transferred into a well of an assay plate and attached on the bottom of the well by centrifugation at 2000×*g* for 20 min at 4 °C. After incubation at 37 °C for 10 min, the measurement of oxygen consumption rate was calculated according to the manufacturer's protocol. Injections were as follows: port A, 20 μl of 30 mM ADP (5 mM final); port B, 20 μl of 35 μM oligomycin (5 μM final); port C, 20 μl of 40 μM FCCP (5 μM final); and port D, 20 μl of 90 μM antimycin A (10 μM final) and 18 μM antimycin A (18 μM final). Typical mix and measurement cycle times for the assay were the same as previous reports [38,39].

2.19. Evaluation of oxidative stress

Levels of hydrogen peroxide, 8-hydroxy-2-deoxyguanosine (8-OHdG) and malondialdehyde (MDA) in the PFC were determined with Hydrogen Peroxide Colorimetric Detection Kit (Enzo Life sciences, Inc., NY), EpiQuik 8-OHdG DNA Damage Quantification Direct Kit (Colorimetric) (Epigentek, NY) and OxiSelect TBARS Assay Kit (Cell Biolabs Inc., CA), respectively, according to the manufacturer's protocol.

2.20. Statistical analysis

In the behavioral and biochemical studies, statistical differences between the two groups were determined with a Student's *t*-test. Statistical differences between more than 3 groups were determined using a one-way or two-way ANOVA with repeated measures followed by Tukey's multiple comparisons test. A value of $p < 0.05$ was considered statistically significant.

2.21. Study approval

For all animal studies, the experimental procedures were approved by the Animal Experiment Committee of the Tokyo Metropolitan Institute of Medical Science (approval no. 15001, 16001, 17003, 18006, 19003, 20005).

2.22. Data availability

RNA-seq data are available in the NCBI Gene Expression Omnibus (GEO): accession number is GSE149585 (token: crwvwyysvnipxwz). Also, Custom R codes and data to support the analysis, visualizations, functional and gene set enrichments are available at: https://github.com/konopkalab/Glo1_Vitamin.

3. Results

3.1. Generation of Glo1 knockout mouse

We generated *Glo1* KO mice by gene trapping (Fig. 1A) and confirmed the insertion of the gene-trap cassette into the *Glo1* gene by PCR (Fig. 1B). We confirmed *Glo1* mRNA decreased to approximately 50% and 0% in the *Glo1* HE and KO mice, respectively, without any changes in gene expression of other enzymes for MG detoxification such as glyoxalase 2 (*Glo2*) and aldo-keto reductase (*Akr*) (Fig. 1C). We also determined the loss of the GLO1 protein in various organs and brain regions of *Glo1* KO mice (Fig. 1D and E) and loss of GLO1 enzymatic activity in the whole brain of *Glo1* KO mice (Fig. 1F). Furthermore, the body weight in *Glo1* KO mice was significantly decreased in both sexes compared with WT mice (Fig. 1G).

Next, we assessed behavioral performances of *Glo1* KO mice to evaluate the effect of impairment of glyoxalase system on mouse behaviors. The *Glo1* KO mice showed shortened immobility time in the

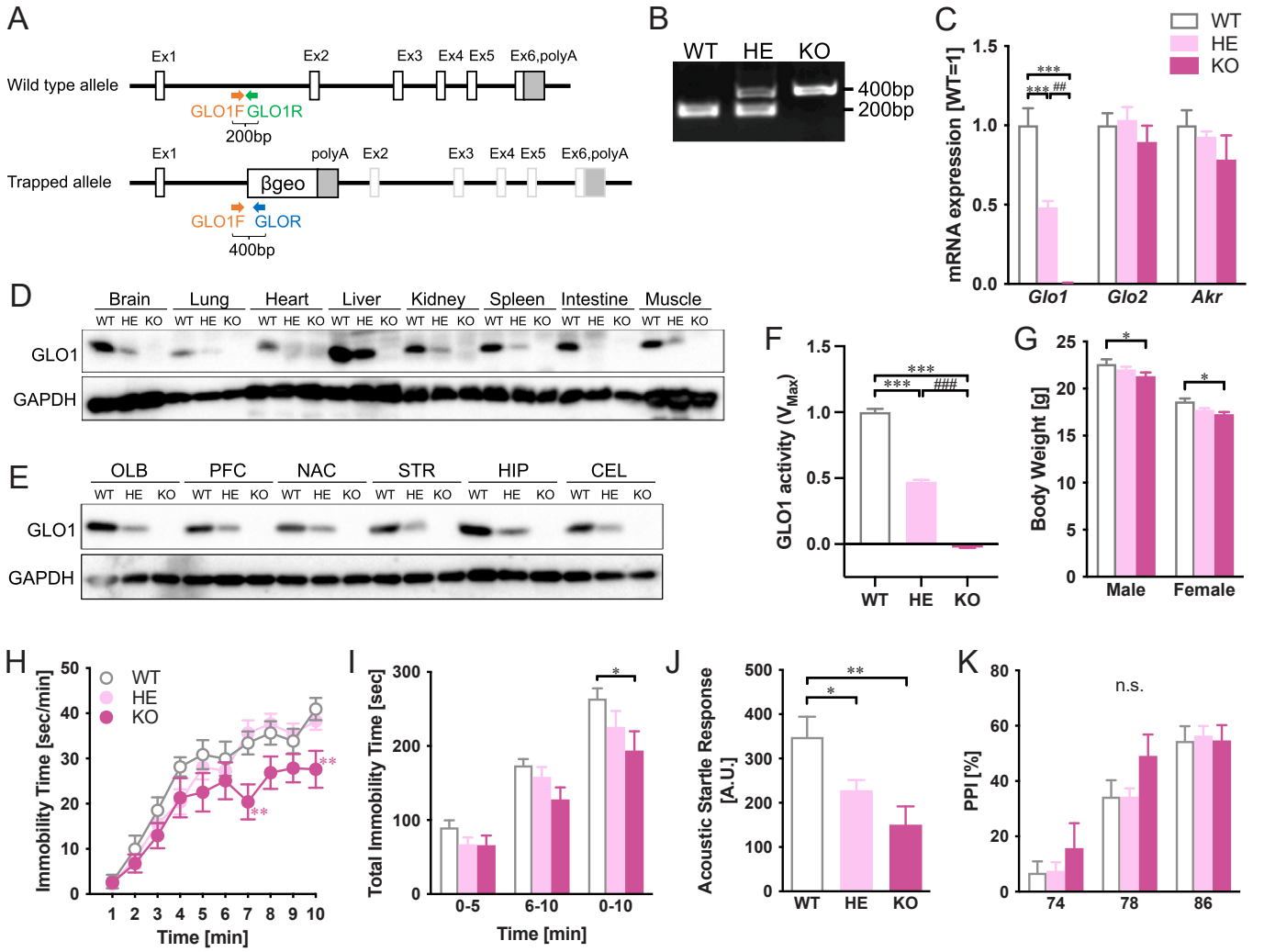

Fig. 1. Generation of Glo1 knockout mice. (A) An overview of *Glo1* gene trapping and (B) PCR for genotyping are shown. (C) mRNA expression in the whole brain was quantified by qPCR (n = 4). Two-way ANOVA: $F_{Interaction(4,18)} = 13.7$, $p < 0.0001$; $F_{Gene(2,18)} = 46.4$, $p < 0.0001$; $F_{Genotype(2,\ 9)} = 9.88$, $p < 0.01$. In the various organs (D) and each brain regions (E), protein level of GLO1 is shown by western blotting using an anti-GLO1 antibody (Clone 6F10, Sigma) and anti-GAPDH (6C5, Santa cruz). (F) GLO1 activity was measured in whole brain (n = 3). One-way ANOVA: $F_{(2,6)} = 880$, $p < 0.0001$. (G) Body weight was measured at 8 weeks (n = 7–19). Two-way ANOVA: $F_{Interaction(2,64)} = 0.168$, $p > 0.05$; $F_{Sex(1,64)} = 250$, $p < 0.0001$; $F_{Genotype(2,\ 64)} = 7.26$, $p < 0.01$. In the forced swimming test, (H) the time course and (I) total scores of the immobility time are shown. Two-way ANOVA: (H) $F_{Interaction(18,\ 396)} = 1.89$; $p < 0.05$, $F_{Time(9,\ 396)} = 75.9$; $p < 0.0001$, $F_{Genotype(2,\ 44)} = 3.35$; $p < 0.05$, (I) $F_{Interaction(4,\ 92)} = 2.08$; $p > 0.05$, $F_{Time(2,\ 92)} = 248$; $p < 0.0001$, $F_{Genotype(2,\ 46)} = 2.16$; $p = 0.13$. In the prepulse inhibition test, (J) acoustic startle response without prepulse [One-way ANOVA: $F_{(2,\ 41)} = 6.91$, $p < 0.01$.] and (K) prepulse inhibition [Two-way ANOVA: $F_{Interaction(4,\ 84)} = 2.41$; $p > 0.05$, $F_{Prepulse(2,\ 84)} = 183$; $p < 0.0001$, $F_{Genotype(2,\ 42)} = 0.35$; $p > 0.05$.] are shown. $^{*}p < 0.05$, $^{**}p < 0.01$, $^{***}p < 0.001$, $^{\#\#}p < 0.01$ and $^{\#\#\#}p < 0.001$. OLB: olfactory bulb, PFC: prefrontal cortex, NAC: nucleus accumbens, STR: striatum, HIP: hippocampus, CEL: cerebellum.

forced swimming test (FST) (Fig. 1H and I) and less acoustic startle response in the prepulse inhibition (PPI) test without changes in PPI score (Fig. 1J and K). However, the *Glo1* KO mice showed almost no changes in many behavioral tests, such as open-field test, social interaction tests, Y-maze test and novel object recognition test (Suppl. Fig. S1). These findings suggest that gene deletion of *Glo1* alone is insufficient to cause schizophrenia-like behaviors.

3.2. Combined effects of Glo1 KO and VB6 deficiency on methylglyoxal levels in the brain and mouse behaviors

Next, we sought to develop a novel *in vivo* model for schizophrenia by an add-on treatment with an environmental factor, VB6 deficiency observed in more than 35% patients with schizophrenia [7,10,40], to the *Glo1* KO mice. We fed the *Glo1* KO and WT mice a VB6-lacking diet containing low VB6 at 5 μg/100 g pellets from 8 to 12 weeks of age. We fed control mice a normal diet in which VB6 was present at 1.4 mg/100 g pellets. *Glo1* KO mice with the normal diet (KO/VB6(+)) showed lower plasma VB6 levels than WT mice with the normal diet (WT/VB6(+)), suggesting that *Glo1* deletion slightly decreases plasma VB6 levels. After feeding with the VB6-lacking diet for 4 weeks, we confirmed that plasma VB6 levels in WT (WT/VB6(−)) and KO (KO/VB6(−)) mice significantly decreased (Fig. 2A), although there is no change between them. Feeding with the VB6-lacking diet decreased body weight in both WT and KO mice (Fig. 2B). Furthermore, we measured homocysteine level in the plasma of these mice, since VB6 deficiency is well known to elevate homocysteine via dysfunction of VB6-dependent enzymes [41]. We found that plasma homocysteine level in KO/VB6(−) mice significantly increased compared with that in WT/VB6(+) mice (Fig. 2C). We also determined that the VB6 deficiency is a cause of the accumulated homocysteine in the plasma (Two-way ANOVA: p = 0.006), although there was no significant difference between WT/VB6(−) and WT/VB6(+) mice.

To evaluate the effect of GLO1 dysfunction and VB6 deficiency on the

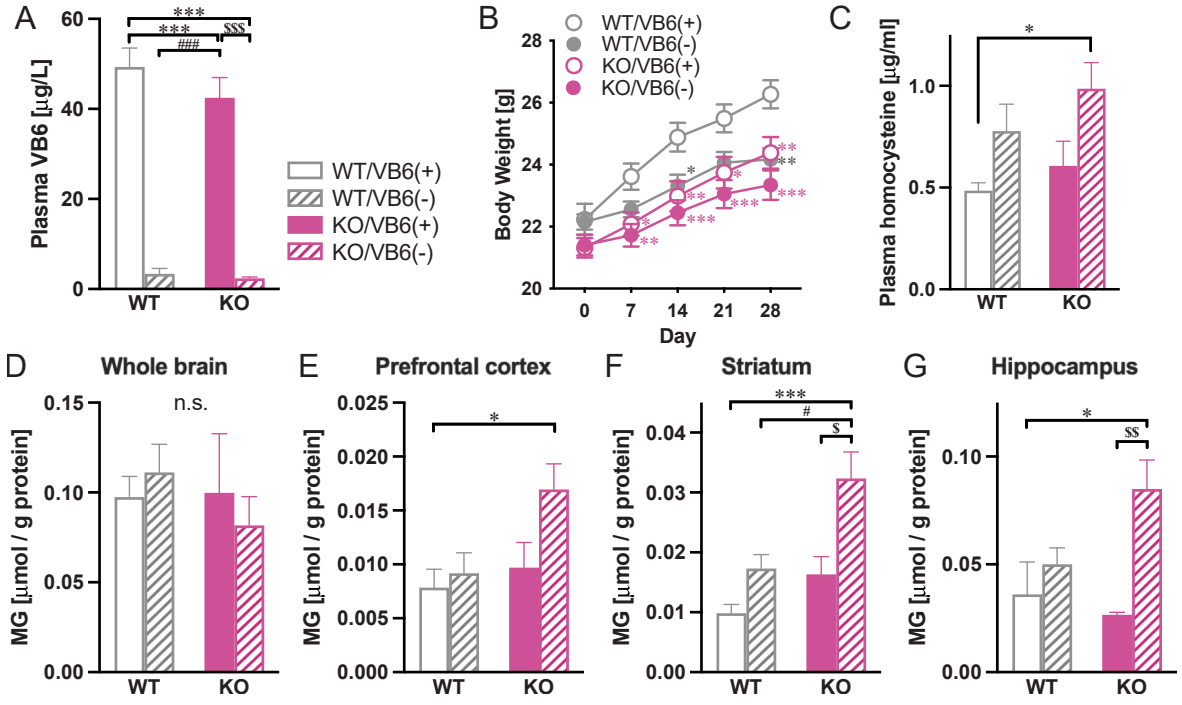

Fig. 2. Development of Glo1 KO x VB6 deficiency mice. *Glo1* WT and KO mice were fed with VB6-lacking (VB6(−)) or control diet (VB6(+)) from 8 to 12 weeks. (A) VB6 levels (n = 27) were determined. (B) Changes in body weight during feeding with VB6(+) or VB6(−) diet are indicated (n = 14–18). (C) Homocysteine levels in the plasma were quantified (n = 8). Methylglyoxal levels were measured in (D) whole brain, (E) PFC, (F) STR and (G) HIP (n = 5). Two-way ANOVA: (A) $F_{Interaction(1,104)} = 0.87$, $p > 0.05$; $F_{Genotype(1,104)} = 1.57$, $p > 0.05$; $F_{VB6(1,104)} = 186$, $p < 0.0001$, (B) $F_{Interaction(12, 232)} = 6.28$; $p < 0.0001$, $F_{Day(4, 232)} = 212$; $p < 0.0001$, $F_{Group(3, 58)} = 5.53$; $p < 0.01$, (C) $F_{Interaction(1,28)} = 0.15$, $p > 0.05$; $F_{Genotype(1,28)} = 2.18$, $p > 0.05$; $F_{VB6(1,28)} = 9.05$, $p < 0.01$, (D) $F_{Interaction(1, 16)} = 0.60$; $p > 0.05$, $F_{Genotype(1, 16)} = 0.43$; $p < 0.05$, $F_{VB6(1, 16)} = 0.01$; $p > 0.05$, (E) $F_{Interaction(1, 16)} = 2.01$; $p > 0.05$, $F_{Genotype(1, 16)} = 5.26$; $p < 0.05$, $F_{VB6(1, 16)} = 4.19$; $p > 0.05$, (F) $F_{Interaction(1, 16)} = 2.03$; $p > 0.05$, $F_{Genotype(1, 16)} = 12.8$; $p < 0.01$, $F_{VB6(1, 16)} = 15.2$; $p < 0.01$, (G) $F_{Interaction(1, 16)} = 4.22$; $p > 0.05$, $F_{Genotype(1, 16)} = 1.38$; $p > 0.05$, $F_{VB6(1, 16)} = 11.2$; $p < 0.01$. $^{*}p < 0.05$, $^{**}p < 0.01$, $^{***}p < 0.001$, $^{\#}p < 0.05$, $^{\#\#\#}p < 0.001$, $^{\$}p < 0.05$, $^{\$\$}p < 0.01$ and $^{\$\$\$}p < 0.001$.

MG levels, we quantified MG in various brain regions of *Glo1* KO mice with VB6 deficiency. The MG levels in the prefrontal cortex (PFC: Fig. 2E), the striatum (STR: Fig. 2F) and the hippocampus (HIP: Fig. 2G) of the KO/VB6(−) group significantly increased compared to the WT/VB6(+) group, although there is no change in the whole brain (Fig. 2D) and other brain areas (Suppl. Fig. S2). There were no changes in MG levels in the WT/VB6(−) and KO/VB6(+) groups relative to the WT/VB6(+) group in all brain regions, suggesting that the accumulation of MG isn't caused by *Glo1* gene deletion or VB6 deficiency alone, but by the combination of them.

Moreover, to investigate whether GLO1 dysfunction and VB6 deficiency affect the function of monoaminergic neuronal systems resulting in the behavioral impairments, we determined monoamines and their metabolites in various regions of the brain (Suppl. Fig. S3) and found that there were no changes in dopamine, noradrenaline (NA), or serotonin across all brain regions of KO/VB6(−) mice. We also demonstrated that 3-methoxy-4-hydroxyphenylglycol (MHPG) levels markedly increased in the VB6-deficient groups, WT/VB6(−) and KO/VB6(−), leading to enhanced NA turnover. This is in line with previous reports that VB6 deficiency induces the enhancement of NA metabolism (Suppl. Figs. S3G and S3H), although the differences were not significant.

Next, we assessed the behavioral performances of *Glo1* KO mice with VB6 deficiency. The VB6 deficient groups, WT/VB6(−) and KO/VB6(−), showed less locomotor activity in the first 10 min (Fig. 3A). In the novel object recognition test, the VB6 deficient groups also showed decreased exploratory preference during the retention session compared with the VB6 normal groups, although there was no change in exploratory time (Fig. 3B and C). In a social interaction test using a 3-chamber apparatus, the VB6 deficient groups spent less time in the chamber with an unfamiliar mouse and had decreased interaction time during the test session compared to the WT/VB6(+) group (Fig. 3D and E). These data demonstrate that the VB6-deficient mice display behavioral deficits of sociability and cognitive memory. Moreover, similar to the results in Fig. 1H–K, the *Glo1* KO, KO/VB6(+), and KO/VB6(−) groups showed shortened immobility time in the FST (Fig. 3F and G) and less acoustic startle response in the PPI test (Fig. 3H). However, these behavioral abnormalities observed in the *Glo1* KO groups did not worsen with the combination of VB6 deficiency. Finally, the PPI deficit was only observed in the KO/VB6(−) group (Fig. 3I), suggesting that sensorimotor deficits occur only when the GLO1 dysfunction is combined with VB6 deficiency.

3.3. *Differential gene expression analysis in the brain of Glo1 KO x VB6-deficient mice*

To identify molecular pathways impaired by *Glo1* KO and VB6 deficiency in the brain, we carried out RNA-seq in the PFC, STR, and HIP, where MG significantly accumulated in KO/VB6(−) mice (Suppl. Table S1). We identified only one differentially expressed gene (DEG), *Igf2*, in the PFC and STR, not HIP, by comparison between WT/VB6(+) vs WT/VB6(−), indicating the effect of the VB6 deficiency alone was minimal (Fig. 4A; Suppl. Table S2). We identified more DEGs by comparing WT/VB6(+) vs KO/VB6(+), indicating a greater effect of the *Glo1* deletion alone (Fig. 4B). Common DEGs in the three brain regions were *Glo1* and three zinc finger proteins (*Zfp40*, *Zfp758,* and *Zfp983*). Moreover, we identified many more DEGs in all brain regions by comparing WT/VB6(+) vs KO/VB6(−), reflecting the enhanced combined effect of the VB6 deficiency and the *Glo1* deletion (Fig. 4C). There were 10 common DEGs in the PFC, STR, and HIP (*Glo1, Zfp40, Atp6v0c, Zfp758, Pla2g7, Zfp983, Decr2, Rps2, Gnptg,* and *Zfp760*). It should be noted that the DEGs in the PFC were markedly increased to 286 genes compared with the other regions, suggesting that the combination of

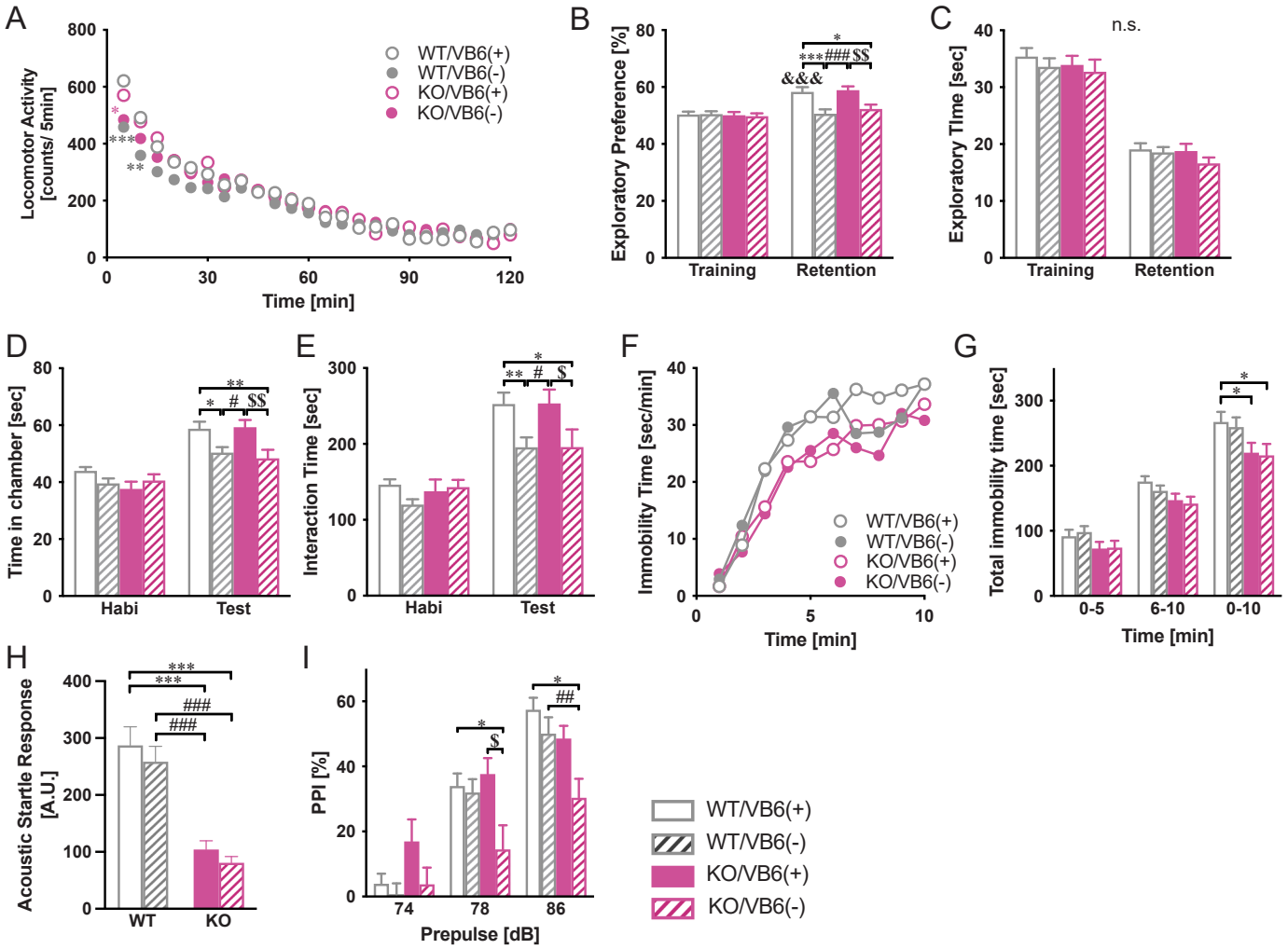

Fig. 3. Behavioral deficits in Glo1 KO x VB6 deficient mice. (A) Time course of locomotor activity in the *Glo1* KO x VB6 deficiency mice were measured. (B) Exploratory preference and (C) exploratory time in the novel object recognition test, (D) time spent in the chamber and (E) interaction time in the social interaction test, (F) the time course and (G) total scores of the immobility time in the forced swimming test, and (H) the acoustic startle response without prepulse and (I) prepulse inhibition (PPI) score in the PPI test were measured. Two-way ANOVA: (A) $F_{\text{Interaction}(69,\ 1863)} = 1.56$; $p < 0.01$, $F_{\text{Time}(23,\ 1863)} = 142$; $p < 0.0001$, $F_{\text{Group}(3,\ 81)} = 0.39$; $p > 0.05$, (B) $F_{\text{Interaction}(3,\ 80)} = 5.53$; $p < 0.01$, $F_{\text{Session}(1,\ 80)} = 27.4$; $p < 0.0001$, $F_{\text{Group}(3,\ 80)} = 5.00$; $p < 0.01$, (C) $F_{\text{Interaction}(3,\ 80)} = 0.12$; $p > 0.05$, $F_{\text{Session}(1,\ 80)} = 271$; $p < 0.0001$, $F_{\text{Group}(3,\ 80)} = 1.00$; $p > 0.05$, (D) $F_{\text{Interaction}(3,\ 80)} = 2.97$; $p < 0.05$, $F_{\text{Session}(1,\ 80)} = 69.5$; $p < 0.0001$, $F_{\text{Group}(3,\ 80)} = 5.19$; $p < 0.01$, (E) $F_{\text{Interaction}(3,\ 80)} = 2.07$; $p > 0.05$, $F_{\text{Session}(1,\ 80)} = 82.7$; $p < 0.0001$, $F_{\text{Group}(3,\ 80)} = 4.40$; $p < 0.01$, (F) $F_{\text{Interaction}(27,\ 702)} = 0.99$; $p > 0.05$, $F_{\text{Time}(9,\ 702)} = 68.5$; $p < 0.0001$, $F_{\text{Group}(3,\ 78)} = 2.47$; $p = 0.068$, (G) $F_{\text{Interaction}(6,\ 156)} = 1.63$; $p > 0.05$, $F_{\text{Genotype}(2,\ 156)} = 497$; $p < 0.0001$, $F_{\text{VB6}(3,\ 78)} = 2.73$; $p < 0.05$, (H) $F_{\text{Interaction}(1,\ 79)} = 0.01$; $p > 0.05$, $F_{\text{Genotype}(1,\ 79)} = 47.3$; $p < 0.0001$, $F_{\text{VB6}(1,\ 79)} = 0.98$; $p < 0.05$, (I) $F_{\text{Interaction}(6,\ 158)} = 3.99$; $p < 0.01$, $F_{\text{Prepulse}(2,\ 158)} = 136$; $p < 0.0001$, $F_{\text{Group}(3,\ 79)} = 3.94$; $p < 0.05$. $^{*}p < 0.05$, $^{**}p < 0.01$, $^{***}p < 0.001$, $^{\#}p < 0.05$, $^{\#\#}p < 0.01$, $^{\#\#\#}p < 0.001$, $^{\$}p < 0.05$ and $^{\$\$}p < 0.01$.

VB6 deficiency and the *Glo1* deletion has a greater impact on gene expression in the PFC.

Cell type gene enrichment analysis indicated that the 286 DEGs in the PFC, 70 up-regulated and 216 down-regulated genes, were enriched for genes expressing specifically in endothelial cells and glial cells rather than neurons (Fig. 4D; Suppl. Table S3). The 286 DEGs were also enriched with genes in an asdM16 module, which is related to autism spectrum disorder (ASD), and enriched for genes involved in immune and inflammatory responses [30], but was not enriched for schizophrenia related genes (Fig. 4E). The enrichment results for the 286 DEGs are driven by the down-regulated genes, because the results of the down-regulated genes were the same as those of the 286 DEGs. To further examine the relationship between the PFC DEGs and dysregulation in neuropsychiatric disorders, we used modules associated with schizophrenia, autism, or bipolar disorder [36]. We found that down-regulated genes are overrepresented for genes in a mitochondria-related module severely downregulated in schizophrenia (M33), an astrocyte module upregulated in autism and schizophrenia (M3), and a microglia module downregulated in schizophrenia (M15). These results further underscore the role of combination of GLO1 dysfunction and VB6 deficiency in schizophrenia etiologies and highlight the link between glial cells and neuropsychiatric disease etiologies (Fig. 4F).

Gene ontology (GO) analysis of the down-regulated DEGs identified enrichment for mitochondria-related function pathways, such as "Mitochondrial envelop," "Mitochondrion," and "Respiratory chain complex" (Fig. 4G), whereas that of the up-regulated genes enriched with "Whole membrane" only. Taken together, these findings suggest that the combination of VB6 deficiency and the *Glo1* deletion may impair gene expressions in endothelial and glial cells and induce mitochondrial dysfunction in the PFC.

3.4. *Weighted gene co-expression network analysis (WGCNA) and mitochondrial function in the PFC*

To further identify gene co-expression modules in the PFC impaired

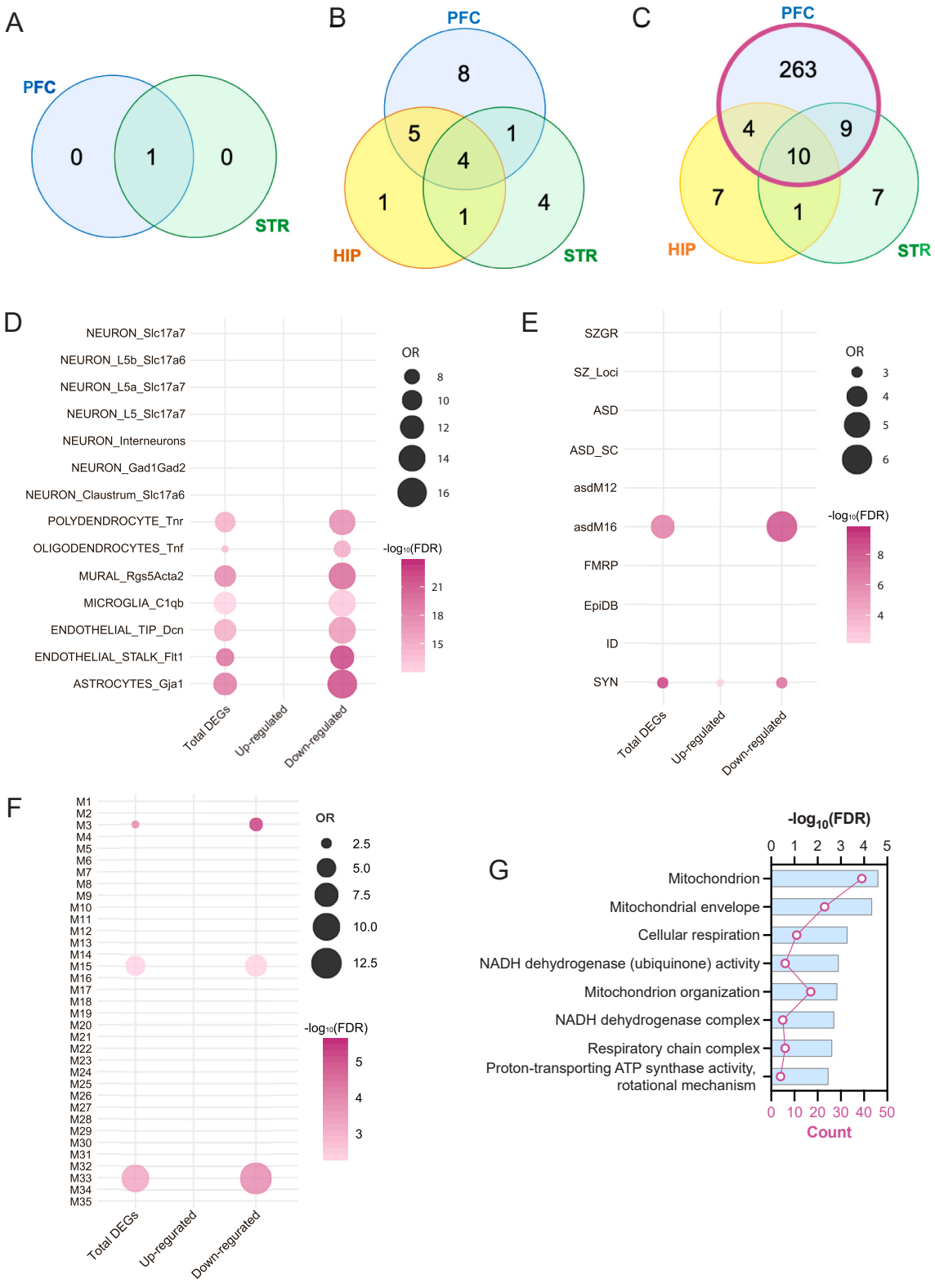

Fig. 4. Changes of gene expression in the brain of Glo1 KO x VB6 deficiency mice Venn diagrams of differentially expression genes (DEGs) overlapped among the PFC, STR, and HIP. (A) WT/VB6(−), (B) KO/VB6(+) and (C) KO/VB6(−) compared with WT/VB6(+) are shown. Gene set enrichment between DEGs in the PFC of KO/VB6(−) mice and (D) cell type markers from single-nuclei RNA-seq, (E) disease risk genes, or (F) modules associated with psychiatric disorders. Enrichment analyses were performed using a Fisher's exact test. Odds ratios (OR) and -$\log_{10}$(FDR) are shown. (G) GO analyses of 216 down-regulated DEGs in the PFC between WT/VB6(+) and KO/VB6(−).

by the combination of VB6 deficiency and *Glo1* deletion, we performed weighted gene co-expression network analysis (WGCNA) [26] (Fig. 5A; Suppl. Table S4). We found two modules, "lightcyan" and "green-yellow", that were associated with the combination of VB6 deficiency and *Glo1* deletion. The lightcyan module showed enrichment with DEGs in the PFC as well as mitochondria-related genes (Fig. 5B–D). GO analysis using the lightcyan module significantly identified enrichment for mitochondrial function (Fig. 5E). Considering that GO analysis using 286 DEGs in the PFC also identified enrichment for mitochondria-related functional pathways, these results suggest a hypothesis that altered gene expression may affect mitochondrial function in the PFC of the KO/VB6(−) mice.

To test the hypothesis, we evaluated respiratory function of mitochondria isolated from the PFC in the *Glo1* KO mice with VB6 deficiency using a flux analyzer. We found that the oxygen consumption rates in the KO/VB6(−) mice were significantly decreased compared with the WT/VB6(+) (Fig. 6A). Moreover, we demonstrated enhanced oxidative stress markers with the mitochondrial dysfunction in the PFC, such as hydrogen peroxide, an oxidative DNA damage marker 8-OHdG and a lipid peroxidation marker MDA (Fig. 6B–D). Together, these results indicate that the combination of VB6 deficiency and the *Glo1* deletion impaired mitochondrial respiratory function via aberrant gene expression, leading to enhanced oxidative stress in the PFC.

4. Discussion

In a previous report, we identified novel *GLO1* mutations that reduce enzymatic activity in patients with schizophrenia [7]. To identify the mechanism of *GLO1* gene deletion on brain function, we first generated *Glo1* KO mice and evaluated behavioral phenotypes (Fig. 1). However, the *Glo1* KO mice showed few behavioral changes related to schizophrenia (Fig. 1 and Suppl. Fig. S1). Moreover, we also confirmed that the *Glo1* KO alone did not increase MG levels in the brain (Fig. 2D–G and Suppl. Fig. S2). These findings imply that other compensatory systems remove MG in *Glo1* KO mice. For example, other enzymes such as aldehyde dehydrogenase and AKR metabolize MG to pyruvate and hydroxyacetone, respectively [42,43]. Consistent with our findings, *in vitro* and *in vivo* studies show that in the absence of *Glo1*, AKR may compensate concerning MG detoxification, resulting in no MG accumulation [44,45]. We also found no change in gene expression of AKR in the brain of *Glo1* KO mice (Fig. 1C). This suggests that the catabolic enzyme might compensate for the elimination of MG, which is usually removed by the glyoxalase system.

The *Glo1* KO mice exhibited shortened immobility time in the FST, a behavior associated with antidepressant-like behavior (Fig. 1H and I). This is consistent with a recent study that GLO1 inhibitors are useful as novel antidepressants [46]. Two structurally distinct GLO1 inhibitors decreased the immobility time in the FST and ameliorated the stress-induced depression-like behavior. Furthermore, the treatment

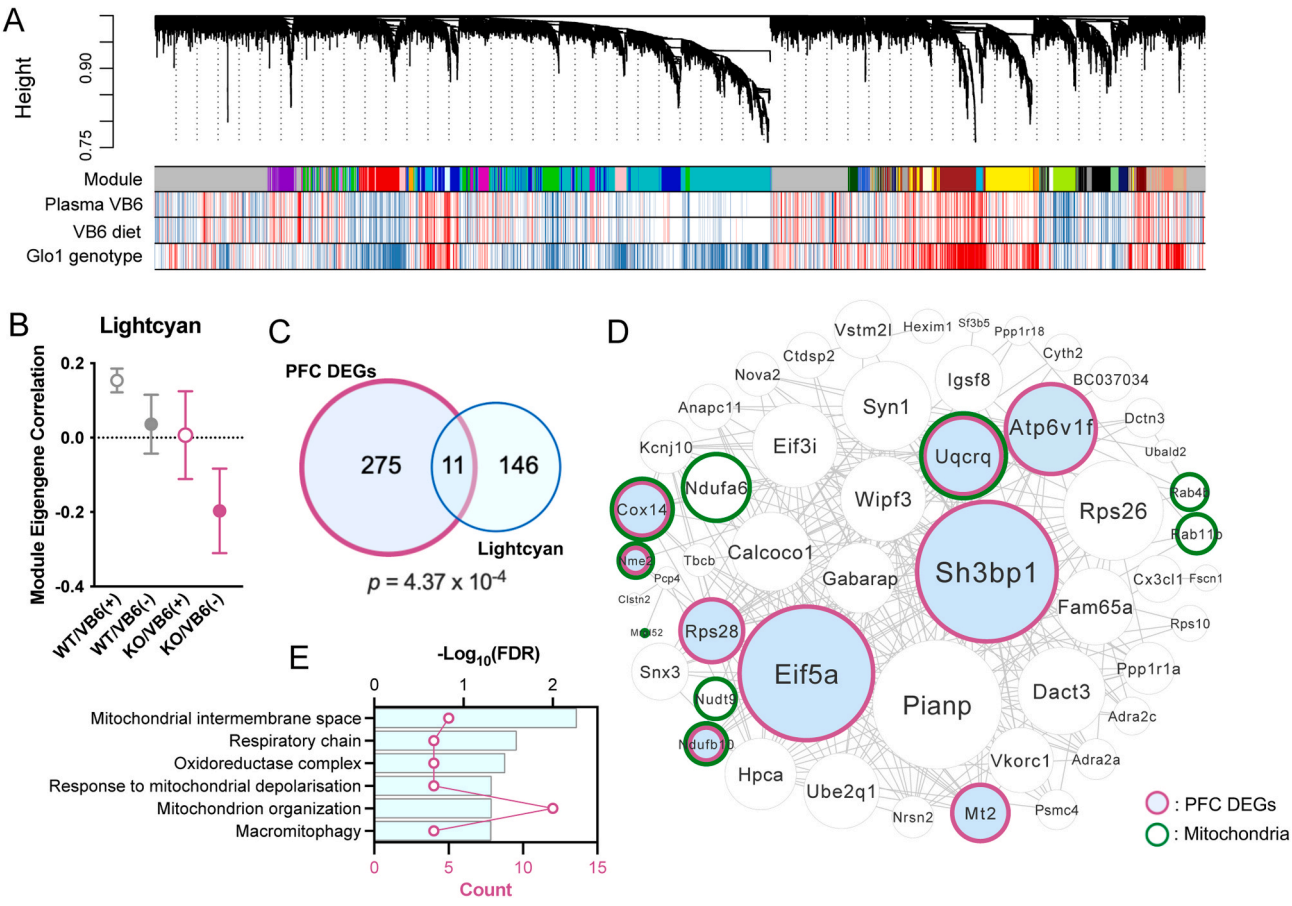

Fig. 5. Weighted gene co-expression network analysis (WGCNA) and mitochondrial function in the PFC. (A) Representative network dendrograms. (B) Module eigengene (ME) of the lightcyan module significantly associated with the KO/VB6(−) group. SEs are calculated based on the eigengene across samples. Dots represent the mean eigengene for that module. (C) Venn diagrams of genes overlapped between the lightcyan module and DEGs in the PFC of KO/VB6(−) are shown [$p = 4.37 \times 10^{-4}$; hypergeometric test]. (D) Visualization of the top 250 connections ranked by weighted topological overlap values for the lightcyan module. Node size corresponds to the number of edges (degree). DEGs in the PFC are highlighted in blue and surrounded by a purple frame. Mitochondria-related genes are surrounded by a green frame. (E) GO analysis of genes in the lightcyan is shown. . (For interpretation of the references to color in this figure legend, the reader is referred to the Web version of this article.)

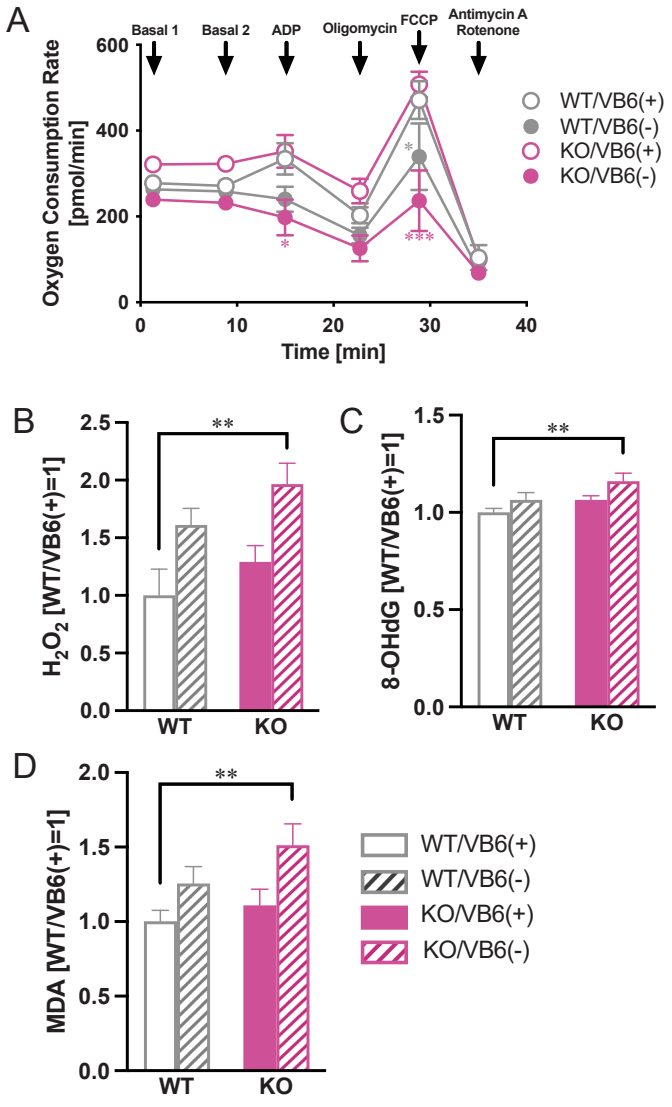

Fig. 6. Mitochondrial Respiratory dysfunction and enhanced oxidative stress in the PFC of Glo1 KO x VB6 deficiency mice. (A) Oxygen consumption rates of mitochondrial isolated from the PFC are measured by a flux analyzer. Oxidative stress markers including (B) hydrogen peroxide, (C) 8-OHdG and (D) MDA are quantified in the PFC. Two-way ANOVA: (A) $F_{\text{Interaction}(15,\ 80)} = 2.11$; $p < 0.05$, $F_{\text{Time}(5,\ 80)} = 54.0$; $p < 0.0001$, $F_{\text{Group}(3,\ 16)} = 9.93$; $p < 0.001$ (n = 5). (B) $F_{\text{Interaction}(1,\ 20)} = 0.03$; $p > 0.05$, $F_{\text{Genotype}(1,\ 20)} = 3.32$; $p > 0.05$, $F_{\text{VB6}(1,\ 20)} = 13.2$; $p < 0.01$ (n = 6). (C) $F_{\text{Interaction}(1,\ 20)} = 0.24$; $p > 0.05$, $F_{\text{Genotype}(1,\ 20)} = 6.50$; $p < 0.05$, $F_{\text{VB6}(1,\ 20)} = 6.32$; $p < 0.05$ (n = 6). (D) $F_{\text{Interaction}(1,\ 20)} = 0.44$; $p > 0.05$, $F_{\text{Genotype}(1,\ 20)} = 2.63$; $p > 0.05$, $F_{\text{VB6}(1,\ 20)} = 8.64$; $p < 0.01$. *$p < 0.05$, **$p < 0.01$ and ***$p < 0.001$ (n = 6).

with the GLO1 inhibitors increased the expression of molecular markers of the antidepressant response, including brain-derived neurotrophic factor (BDNF) and cyclic-AMP response-binding protein (CREB) phosphorylation in the HIP and the medial PFC. Considering our result that *Glo1* gene deletion alone is insufficient to increase MG levels in the brain, the therapeutic effect of the GLO1 inhibitors and the antidepressant-like behavior in the *Glo1* KO mice is probably independent of MG accumulation.

Next, to develop a mouse model that further recapitulates the pathology of schizophrenia, we depleted VB6 in the *Glo1* KO mice by feeding them VB6(−) diets. We found that the KO/VB6(−) mice displayed an accumulation of MG in the PFC, HIP, and STR (Fig. 2D–G). Considering that VB6 is known to directly scavenge MG and trap ROS [47,48], it is plausible that the combination of VB6 deficiency with GLO1 dysfunction can accumulate MG in the brain. Moreover, the KO/VB6(−) mice showed behavioral deficits, such as social deficits, cognitive impairment, and a sensorimotor deficit in the PPI test (Fig. 3). Moreover, RNA-seq expression analysis revealed a marked increase in DEGs in the PFC by the combination of *Glo1* gene deletion and VB6 deficiency (Fig. 4A–C). Gene enrichment analysis showed that the 286 DEGs in the PFC were enriched with genes expressing specifically in endothelial cells and glial cells, but not neurons (Fig. 4D). An association between PPI deficits observed in KO/VB6(−) mice and glial cell damage may fit with previous reports. For example, the expression of astrocytic markers is variable in the PFC of a mouse model for schizophrenia showing PPI impairment [49]. Cortical myelination by oligodendrocytes correlates with PPI deficits [50]. Furthermore, chimeric mice of glia cells differentiated from induced pluripotent stem (iPS) cells derived from patients with schizophrenia displayed PPI deficits [51]. These findings suggest that glial cells may be impaired in the subpopulation of schizophrenic patients with GLO1 dysfunction and VB6 deficiency.

We performed WGCNA analysis and found that the gene co-expression module “lightcyan” associated with mitochondrial function in the PFC of KO/VB6(−) mice (Fig. 5A–E). Since enrichment and GO analysis using DEGs also revealed mitochondrial dysfunction (Fig. 4G), we isolated mitochondria from the PFC of KO/VB6(−) mice and found that oxidative phosphorylation was impaired (Fig. 6A). Mitochondrial dysfunction has been frequently reported in patients with schizophrenia [52]. Several studies using postmortem brains demonstrated a decrease in the activity of complex IV in the PFC of patients with schizophrenia [53], and a global down-regulation of mitochondria-related genes by microarray analysis [54]. Also, mitochondrial dysfunction has also been found in patient-derived iPS cells [55,56]. These findings suggest that the combination of GLO1 dysfunction and VB6 deficiency may affect mitochondrial function in KO/VB6(−) mice, causing schizophrenia-like sensorimotor deficits.

In the present study, significant changes in gene expression were observed only in the PFC of KO/VB6(−) mice, even though the MG accumulation was observed not only in the PFC but also in the STR and the HIP. These findings suggest that the aberrant gene expression in the PFC might occur independently of MG accumulation. The aberrant gene expression observed in the PFC of KO/VB6(−) mice suggests the disturbance of the respiratory chain (Fig. 6A). On the other hand, MG can also disrupt mitochondrial respiration; incubation of isolated mitochondria with MG produced a concentration-dependent decrease in state III as well as an increase and then a decrease in state IV respiration [57]. These findings suggest that mitochondrial dysfunction can be caused by both the aberrant gene expression related to mitochondria and the MG accumulation. Accordingly, the oxidative stress in the PFC of KO/VB6(−) mice would be enhanced, since the disturbance of the respiratory chain leads to the production of oxidative stress [58]. In fact, we found higher expression of oxidative stress markers (Fig. 6B–D). A mouse model for enhanced oxidative stress by deficits of the glutathione antioxidative system showed sensorimotor deficits in the PPI test, which is consistent with our findings [59]. Also, accumulating evidence indicates that oxidative damage exists in schizophrenia [60]. These findings suggest that behavioral deficits shown in the KO/VB6(−) mice might be caused by oxidative stress in the PFC.

VB6 deficiency impairs the transsulfuration pathway via dysfunction of VB6-dependent enzymes such as cystathionine β-synthase and cystathione γ-lyase, resulting in hyperhomocysteinemia [41]. Here, we demonstrated that VB6 deficiency enhanced homocysteine levels in plasma (Fig. 2C). Animal models chronically administered with homocysteine have shown mitochondrial dysfunction and increased oxidative stress in the brain [61–63]. These findings suggest that homocysteine accumulation related to VB6 deficiency might also contribute to the mitochondrial dysfunction and the enhanced oxidative stress in KO/VB6(−) mice, in addition to the aberrant gene expression related to mitochondria and the MG accumulation we observed.

There have also been a number of reports on the association between

homocysteine accumulation and schizophrenia, including our previous study [40]. Some meta-analyses have shown enhanced homocysteine in schizophrenic patients [64,65], including first-episode psychotic subjects without medication [66–68] and chronic schizophrenic patients [69]. It has also been estimated that a 5 μmol increase in plasma homocysteine levels is associated with a 70% increase in the risk of developing schizophrenia [64], and homocysteine levels are positively correlated with the severity of negative symptoms [70–73]. Many early case reports noted a genetic syndrome of homocysteinuria causes schizophrenia-like deficiency [74–77], and genetic meta-analyses have also shown that a variant in methylenetetrahydrofolate reductase (MTHFR), one of the causative genes of homocysteinuria, is associated with schizophrenia [64,78]. Betaine, a therapeutic agent of homocysteinuria, has been reported to be therapeutic for mouse models and iPS cell line phenotypes relevant to schizophrenia [79]. These studies strongly suggested that homocysteine accumulation is a pathophysiology of a subset of patients with schizophrenia. Considering that homocysteine accumulation is one of the causes of schizophrenia-like behavioral deficits exhibited by KO/VB6(−) mice, such as the social deficits, cognitive dysfunction and PPI deficits, homocysteine removal may be an effective therapeutic strategy for patients with GLO1 dysfunction and VB6 deficiency.

Also, MG in the bloodstream appears to disrupt the blood-brain barrier, resulting in activation of the inflammatory response [80,81]. Clinical studies have reported that the aberrant inflammation is frequently seen in schizophrenia and related psychoses [82,83]. The fact that the 286 DEGs in the PFC are significantly correlated with AsdM16, which is associated with immune responses (Fig. 4E), and are also significantly enriched for immune-associated genes [GO:0002376, Immune system process, -log10 (p-value) = 1.38] suggests that inflammation may occur in the PFC of KO/VB6(−) mice. Furthermore, AGEs made from MG are also able to activate the immune response through receptors for AGEs (RAGE) [84]. Thus, AGEs produced from the accumulated MG in KO/VB6(−) mice may lead to the activation of inflammation and the behavioral deficits.

We also found that VB6 deficiency alone induced social deficits and cognitive impairment (Fig. 3A–E). We have already linked behavioral deficits induced by VB6 deficiency to enhanced noradrenergic signaling [85]. The VB6-deficient groups WT/VB6(−) and KO/VB6(−) showed a marked increase in MHPG, a metabolite of noradrenaline, in the brain (Suppl. Fig. S3), although the combination of VB6 deficiency and *Glo1* gene deletion did not increase MHPG synergistically. Thus, the noradrenergic system activation by VB6 deficiency would not cause the PPI deficits observed in the KO/VB6(−) mice.

Another module from the WGCNA, the “greenyellow” module, was also associated with the combination of VB6 deficiency and *Glo1* deletion (Suppl. Figs. S4A and S4B). GO analysis of the greenyellow module identified significant enrichment for RNA splicing and microtubule-related pathways (Suppl. Fig. S4C). Thus, we checked differential exon usage using the DEXseq method in our RNA-seq data [86] and identified genes with differential exon usage in the PFC of *Glo1* KO mice with VB6 deficiency (Suppl. Table S5). We also found that the genes with differential exon usage were enriched for synaptic function by GO analysis (Suppl. Fig. S4D). Next, to evaluate synaptic function, we carried out an electrophysiological analysis of the PFC of *Glo1* KO mice with VB6 deficiency. However, the results showed no significant differences in both miniature excitatory postsynaptic current (mEPSC) and miniature inhibitory postsynaptic current (mIPSC) among all groups, although we observed increased mEPSC amplitude in the KO/VB6(+) group and depolarized membrane potential in the KO/VB6(−) (Suppl. Figs. S4E–S4K). These findings suggest that the effect of alternative splicing on synaptic function in the PFC of *Glo1* KO mice with VB6 deficiency might be minimal.

Taken together, we generated *Glo1* KO mice to evaluate the effect of MG detoxification deficits on brain function and found that *Glo1* KO mice fed with VB6(−) diets exhibited an accumulation of homocysteine in plasma and MG in the PFC, STR, and HIP as well as behavioral deficits including sensorimotor deficit. Furthermore, we found altered gene expression involved in mitochondria function in the PFC of the KO/VB6(−) mice. We therefore hypothesize that the aberrant gene expression and the MG accumulation caused respiratory deficits in the mitochondria of the PFC, leading to increased oxidative stress.

Funding and disclosure

We are grateful for the expert technical assistance of Izumi Nohara, Yukiko Shimada, Emiko Hama, Nanako Obata, Mai Hatakenaka, Chikako Ishida, and Ikuyo Kito. We would also like to express our gratitude to Connor Douglas for his proofreading support.

This work was supported by the JSPS Program for Advancing Strategic International Networks to Accelerate the Circulation of Talented Researchers (S2603); JSPS KAKENHI Grant Numbers 16H05380, 17H05930, 18K06977, 19H04887, 20H03608; AMED under Grant Number JP20dm0107088; the Kanae Foundation for the Promotion of Medical Science; The Uehara Memorial Foundation; The Sumitomo Foundation; The SENSHIN Medical Research Foundation.

The authors have declared that no conflict of interest exists.

Appendix A. Supplementary data

Supplementary data to this article can be found online at https://doi.org/10.1016/j.redox.2021.102057.

References

[1] N. Rabbani, P.J. Thornalley, Dicarbonyl stress in cell and tissue dysfunction contributing to ageing and disease, Biochem. Biophys. Res. Commun. 458 (2) (2015) 221–226.

[2] A.R. Hipkiss, On the relationship between energy metabolism, proteostasis, aging and Parkinson’s disease: possible causative role of methylglyoxal and alleviative potential of carnosine, Aging Dis 8 (3) (2017) 334–345.

[3] N. Rabbani, M. Xue, P.J. Thornalley, Methylglyoxal-induced dicarbonyl stress in aging and disease: first steps towards glyoxalase 1-based treatments, Clin. Sci. (Lond.) 130 (19) (2016) 1677–1696.

[4] T. Valente, A. Gella, X. Fernandez-Busquets, M. Unzeta, N. Durany, Immunohistochemical analysis of human brain suggests pathological synergism of Alzheimer’s disease and diabetes mellitus, Neurobiol. Dis. 37 (1) (2010) 67–76.

[5] R. Ramasamy, S.F. Yan, A.M. Schmidt, Advanced glycation endproducts: from precursors to RAGE: round and round we go, Amino Acids 42 (4) (2012) 1151–1161.

[6] P.J. Thornalley, Endogenous alpha-oxoaldehydes and formation of protein and nucleotide advanced glycation endproducts in tissue damage, Novartis Found. Symp. 285 (2007) 229–243, discussion 243-6.

[7] M. Arai, H. Yuzawa, I. Nohara, T. Ohnishi, N. Obata, Y. Iwayama, S. Haga, T. Toyota, H. Ujike, M. Arai, T. Ichikawa, A. Nishida, Y. Tanaka, A. Furukawa, Y. Aikawa, O. Kuroda, K. Niizato, R. Izawa, K. Nakamura, N. Mori, D. Matsuzawa, K. Hashimoto, M. Iyo, I. Sora, M. Matsushita, Y. Okazaki, T. Yoshikawa, T. Miyata, M. Itokawa, Enhanced carbonyl stress in a subpopulation of schizophrenia, Arch. Gen. Psychiatr. 67 (6) (2010) 589–597.

[8] N. Katsuta, T. Ohnuma, H. Maeshima, Y. Takebayashi, M. Higa, M. Takeda, T. Nakamura, S. Nishimon, T. Sannohe, Y. Hotta, R. Hanzawa, R. Higashiyama, N. Shibata, H. Arai, Significance of measurements of peripheral carbonyl stress markers in a cross-sectional and longitudinal study in patients with acute-stage schizophrenia, Schizophr. Bull. 40 (6) (2014) 1366–1373.

[9] Y. Tomioka, S. Numata, M. Kinoshita, H. Umehara, S.-y. Watanabe, M. Nakataki, Y. Iwayama, T. Toyota, M. Ikeda, H. Yamamori, S. Shimodera, A. Tajima, R. Hashimoto, N. Iwata, T. Yoshikawa, T. Ohmori, Decreased serum pyridoxal levels in schizophrenia: meta-analysis and Mendelian randomization analysis, J. Psychiatr. Neurosci. 43 (3) (2018) 194–200.

[10] M. Miyashita, M. Arai, A. Kobori, T. Ichikawa, K. Toriumi, K. Niizato, K. Oshima, Y. Okazaki, T. Yoshikawa, N. Amano, T. Miyata, M. Itokawa, Clinical features of schizophrenia with enhanced carbonyl stress, Schizophr. Bull. 40 (5) (2014) 1040–1046.

[11] A.F. Carvalho, M. Solmi, M. Sanches, M.O. Machado, B. Stubbs, O. Ajnakina, C. Sherman, Y.R. Sun, C.S. Liu, A.R. Brunoni, G. Pigato, B.S. Fernandes, B. Bortolato, M.I. Husain, E. Dragioti, J. Firth, T.D. Cosco, M. Maes, M. Berk, K. L. Lanctot, E. Vieta, D.A. Pizzagalli, L. Smith, P. Fusar-Poli, P.A. Kurdyak, M. Fornaro, J. Rehm, N. Herrmann, Evidence-based umbrella review of 162 peripheral biomarkers for major mental disorders, Transl. Psychiatry 10 (1) (2020) 152.

[12] M. Itokawa, M. Miyashita, M. Arai, T. Dan, K. Takahashi, T. Tokunaga, K. Ishimoto, K. Toriumi, T. Ichikawa, Y. Horiuchi, A. Kobori, S. Usami, T. Yoshikawa, N. Amano, S. Washizuka, Y. Okazaki, T. Miyata, Pyridoxamine: a novel treatment for

schizophrenia with enhanced carbonyl stress, Psychiatr. Clin. Neurosci. 72 (1) (2018) 35–44.
[13] M. Arai, N. Nihonmatsu-Kikuchi, M. Itokawa, N. Rabbani, P.J. Thornalley, Measurement of glyoxalase activities, Biochem. Soc. Trans. 42 (2) (2014) 491–494.
[14] K. Toriumi, A. Mouri, S. Narusawa, Y. Aoyama, N. Ikawa, L. Lu, T. Nagai, T. Mamiya, H.C. Kim, T. Nabeshima, Prenatal NMDA receptor antagonism impaired proliferation of neuronal progenitor, leading to fewer glutamatergic neurons in the prefrontal cortex, Neuropsychopharmacology : official publication of the American College of Neuropsychopharmacology 37 (6) (2012) 1387–1396.
[15] S. Koike, C. Ando, Y. Usui, Y. Kibune, S. Nishimoto, T. Suzuki, Y. Ogasawara, Age-related alteration in the distribution of methylglyoxal and its metabolic enzymes in the mouse brain, Brain Res. Bull. 144 (2019) 164–170.
[16] Y. Ogasawara, R. Tanaka, S. Koike, Y. Horiuchi, M. Miyashita, M. Arai, Determination of methylglyoxal in human blood plasma using fluorescence high performance liquid chromatography after derivatization with 1,2-diamino-4,5-methylenedioxybenzene, J Chromatogr B Analyt Technol Biomed Life Sci 1029–1030 (2016) 102–105.
[17] J.S. Takahashi, V. Kumar, P. Nakashe, N. Koike, H.C. Huang, C.B. Green, T.K. Kim, ChIP-seq and RNA-seq methods to study circadian control of transcription in mammals, Methods Enzymol. 551 (2015) 285–321.
[18] A. Dobin, C.A. Davis, F. Schlesinger, J. Drenkow, C. Zaleski, S. Jha, P. Batut, M. Chaisson, T.R. Gingeras, STAR: ultrafast universal RNA-seq aligner, Bioinformatics 29 (1) (2013) 15–21.
[19] A. Frankish, M. Diekhans, A.M. Ferreira, R. Johnson, I. Jungreis, J. Loveland, J. M. Mudge, C. Sisu, J. Wright, J. Armstrong, I. Barnes, A. Berry, A. Bignell, S. Carbonell Sala, J. Chrast, F. Cunningham, T. Di Domenico, S. Donaldson, I. T. Fiddes, C. Garcia Giron, J.M. Gonzalez, T. Grego, M. Hardy, T. Hourlier, T. Hunt, O.G. Izuogu, J. Lagarde, F.J. Martin, L. Martinez, S. Mohanan, P. Muir, F.C. P. Navarro, A. Parker, B. Pei, F. Pozo, M. Ruffier, B.M. Schmitt, E. Stapleton, M. M. Suner, I. Sycheva, B. Uszczynska-Ratajczak, J. Xu, A. Yates, D. Zerbino, Y. Zhang, B. Aken, J.S. Choudhary, M. Gerstein, R. Guigo, T.J.P. Hubbard, M. Kellis, B. Paten, A. Reymond, M.L. Tress, P. Flicek, GENCODE reference annotation for the human and mouse genomes, Nucleic Acids Res. 47 (D1) (2019) D766–D773.
[20] L. Wang, S. Wang, W. Li, RSeQC: quality control of RNA-seq experiments, Bioinformatics 28 (16) (2012) 2184–2185.
[21] S. Anders, P.T. Pyl, W. Huber, HTSeq–a Python framework to work with high-throughput sequencing data, Bioinformatics 31 (2) (2015) 166–169.
[22] M.D. Robinson, D.J. McCarthy, G.K. Smyth, edgeR: a Bioconductor package for differential expression analysis of digital gene expression data, Bioinformatics 26 (1) (2010) 139–140.
[23] M.I. Love, W. Huber, S. Anders, Moderated estimation of fold change and dispersion for RNA-seq data with DESeq2, Genome Biol. 15 (12) (2014) 550.
[24] J.T. Leek, W.E. Johnson, H.S. Parker, A.E. Jaffe, J.D. Storey, The sva package for removing batch effects and other unwanted variation in high-throughput experiments, Bioinformatics 28 (6) (2012) 882–883.
[25] F. Supek, M. Bosnjak, N. Skunca, T. Smuc, REVIGO summarizes and visualizes long lists of gene ontology terms, PloS One 6 (7) (2011), e21800.
[26] P. Langfelder, S. Horvath, WGCNA: an R package for weighted correlation network analysis, BMC Bioinf. 9 (1) (2008) 559.
[27] P. Shannon, A. Markiel, O. Ozier, N.S. Baliga, J.T. Wang, D. Ramage, N. Amin, B. Schwikowski, T. Ideker, Cytoscape: a software environment for integrated models of biomolecular interaction networks, Genome Res. 13 (11) (2003) 2498–2504.
[28] A. Saunders, E.Z. Macosko, A. Wysoker, M. Goldman, F.M. Krienen, H. de Rivera, E. Bien, M. Baum, L. Bortolin, S. Wang, A. Goeva, J. Nemesh, N. Kamitaki, S. Brumbaugh, D. Kulp, S.A. McCarroll, Molecular diversity and specializations among the cells of the adult mouse brain, Cell 174 (4) (2018) 1015–1030, e16.
[29] S. Banerjee-Basu, A. Packer, SFARI Gene: an evolving database for the autism research community, Dis Model Mech 3 (3–4) (2010) 133–135.
[30] I. Voineagu, X. Wang, P. Johnston, J.K. Lowe, Y. Tian, S. Horvath, J. Mill, R. M. Cantor, B.J. Blencowe, D.H. Geschwind, Transcriptomic analysis of autistic brain reveals convergent molecular pathology, Nature 474 (7351) (2011) 380–384.
[31] T.N. Turner, Q. Yi, N. Krumm, J. Huddleston, K. Hoekzema, F.S. Ha, A.L. Doebley, R.A. Bernier, D.A. Nickerson, E.E. Eichler, denovo-db: a compendium of human de novo variants, Nucleic Acids Res. 45 (D1) (2017) D804–D811.
[32] M. Pirooznia, T. Wang, D. Avramopoulos, D. Valle, G. Thomas, R.L. Huganir, F. S. Goes, J.B. Potash, P.P. Zandi, SynaptomeDB: an ontology-based knowledgebase for synaptic genes, Bioinformatics 28 (6) (2012) 897–899.
[33] P. Jia, J. Sun, A.Y. Guo, Z. Zhao, SZGR: a comprehensive schizophrenia gene resource, Mol. Psychiatr. 15 (5) (2010) 453–462.
[34] J.C. Darnell, S.J. Van Driesche, C. Zhang, K.Y. Hung, A. Mele, C.E. Fraser, E. F. Stone, C. Chen, J.J. Fak, S.W. Chi, D.D. Licatalosi, J.D. Richter, R.B. Darnell, FMRP stalls ribosomal translocation on mRNAs linked to synaptic function and autism, Cell 146 (2) (2011) 247–261.
[35] X. Ran, J. Li, Q. Shao, H. Chen, Z. Lin, Z.S. Sun, J. Wu, EpilepsyGene: a genetic resource for genes and mutations related to epilepsy, Nucleic Acids Res. 43 (Database issue) (2015) D893–D899.
[36] M.J. Gandal, P. Zhang, E. Hadjimichael, R.L. Walker, C. Chen, S. Liu, H. Won, H. van Bakel, M. Varghese, Y. Wang, A.W. Shieh, J. Haney, S. Parhami, J. Belmont, M. Kim, P. Moran Losada, Z. Khan, J. Mleczko, Y. Xia, R. Dai, D. Wang, Y.T. Yang, M. Xu, K. Fish, P.R. Hof, J. Warrell, D. Fitzgerald, K. White, A.E. Jaffe, E.C. Psych, M.A. Peters, M. Gerstein, C. Liu, L.M. Iakoucheva, D. Pinto, D.H. Geschwind, Transcriptome-wide isoform-level dysregulation in ASD, schizophrenia, and bipolar disorder, Science 362 (6420) (2018).
[37] D. Smedley, S. Haider, B. Ballester, R. Holland, D. London, G. Thorisson, A. Kasprzyk, BioMart–biological queries made easy, BMC Genom. 10 (2009) 22.
[38] S. Sakamuri, J.A. Sperling, V.N. Sure, M.H. Dholakia, N.R. Peterson, I. Rutkai, P. S. Mahalingam, R. Satou, P.V.G. Katakam, Measurement of respiratory function in isolated cardiac mitochondria using Seahorse XFe24 Analyzer: applications for aging research, Geroscience 40 (3) (2018) 347–356.
[39] G.W. Rogers, M.D. Brand, S. Petrosyan, D. Ashok, A.A. Elorza, D.A. Ferrick, A. N. Murphy, High throughput microplate respiratory measurements using minimal quantities of isolated mitochondria, PloS One 6 (7) (2011), e21746.
[40] M. Arai, M. Miyashita, A. Kobori, K. Toriumi, Y. Horiuchi, M. Itokawa, Carbonyl stress and schizophrenia, Psychiatr. Clin. Neurosci. 68 (9) (2014) 655–665.
[41] J. Selhub, Homocysteine metabolism, Annu. Rev. Nutr. 19 (1) (1999) 217–246.
[42] D.L. Vander Jagt, B. Robinson, K.K. Taylor, L.A. Hunsaker, Reduction of trioses by NADPH-dependent aldo-keto reductases. Aldose reductase, methylglyoxal, and diabetic complications, J. Biol. Chem. 267 (7) (1992) 4364–4369.
[43] D.L. Vander Jagt, L.A. Hunsaker, Methylglyoxal metabolism and diabetic complications: roles of aldose reductase, glyoxalase-I, betaine aldehyde dehydrogenase and 2-oxoaldehyde dehydrogenase, Chem. Biol. Interact. 143–144 (2003) 341–351.
[44] J. Morgenstern, T. Fleming, D. Schumacher, V. Eckstein, M. Freichel, S. Herzig, P. Nawroth, Loss of glyoxalase 1 induces compensatory mechanism to achieve dicarbonyl detoxification in mammalian schwann cells, J. Biol. Chem. 292 (8) (2017) 3224–3238.
[45] D. Schumacher, J. Morgenstern, Y. Oguchi, N. Volk, S. Kopf, J.B. Groener, P. P. Nawroth, T. Fleming, M. Freichel, Compensatory mechanisms for methylglyoxal detoxification in experimental & clinical diabetes, Mol Metab 18 (2018) 143–152.
[46] K.M.J. McMurray, M.J. Ramaker, A.M. Barkley-Levenson, P.S. Sidhu, P.K. Elkin, M. K. Reddy, M.L. Guthrie, J.M. Cook, V.H. Rawal, L.A. Arnold, S.C. Dulawa, A. A. Palmer, Identification of a novel, fast-acting GABAergic antidepressant, Mol. Psychiatr. 23 (2) (2018) 384–391.
[47] J.M. Onorato, A.J. Jenkins, S.R. Thorpe, J.W. Baynes, Pyridoxamine, an inhibitor of advanced glycation reactions, also inhibits advanced lipoxidation reactions. Mechanism of action of pyridoxamine, J. Biol. Chem. 275 (28) (2000) 21177–21184.
[48] V. Amarnath, K. Amarnath, K. Amarnath, S. Davies, L.J. Roberts, 2nd, Pyridoxamine: an extremely potent scavenger of 1,4-dicarbonyls, Chem. Res. Toxicol. 17 (3) (2004) 410–415.
[49] L. Sun, L. Min, H. Zhou, M. Li, F. Shao, W. Wang, Adolescent social isolation affects schizophrenia-like behavior and astrocyte biomarkers in the PFC of adult rats, Behav. Brain Res. 333 (2017) 258–266.
[50] R. Zhang, J. He, S. Zhu, H. Zhang, H. Wang, A. Adilijiang, L. Kong, J. Wang, J. Kong, Q. Tan, X.M. Li, Myelination deficit in a phencyclidine-induced neurodevelopmental model of schizophrenia, Brain Res. 1469 (2012) 136–143.
[51] M.S. Windrem, M. Osipovitch, Z. Liu, J. Bates, D. Chandler-Militello, L. Zou, J. Munir, S. Schanz, K. McCoy, R.H. Miller, S. Wang, M. Nedergaard, R.L. Findling, P.J. Tesar, S.A. Goldman, Human iPSC glial mouse chimeras reveal glial contributions to schizophrenia, Cell Stem Cell 21 (2) (2017) 195–208 e6.
[52] D. Ben-Shachar, D. Laifenfeld, Mitochondria, synaptic plasticity, and schizophrenia, Int. Rev. Neurobiol. 59 (2004) 273–296.
[53] I. Maurer, S. Zierz, H. Moller, Evidence for a mitochondrial oxidative phosphorylation defect in brains from patients with schizophrenia, Schizophr. Res. 48 (1) (2001) 125–136.
[54] P. Ni, H. Noh, G.H. Park, Z. Shao, Y. Guan, J.M. Park, S. Yu, J.S. Park, J.T. Coyle, D. R. Weinberger, R.E. Straub, B.M. Cohen, D.L. McPhie, C. Yin, W. Huang, H.Y. Kim, S. Chung, iPSC-derived homogeneous populations of developing schizophrenia cortical interneurons have compromised mitochondrial function, Mol. Psychiatr. 25 (11) (2020) 2873–2888.
[55] K. Iwamoto, M. Bundo, T. Kato, Altered expression of mitochondria-related genes in postmortem brains of patients with bipolar disorder or schizophrenia, as revealed by large-scale DNA microarray analysis, Hum. Mol. Genet. 14 (2) (2005) 241–253.
[56] O. Robicsek, R. Karry, I. Petit, N. Salman-Kesner, F.J. Muller, E. Klein, D. Aberdam, D. Ben-Shachar, Abnormal neuronal differentiation and mitochondrial dysfunction in hair follicle-derived induced pluripotent stem cells of schizophrenia patients, Mol. Psychiatr. 18 (10) (2013) 1067–1076.
[57] M.G. Rosca, V.M. Monnier, L.I. Szweda, M.F. Weiss, Alterations in renal mitochondrial respiration in response to the reactive oxoaldehyde methylglyoxal, Am. J. Physiol. Ren. Physiol. 283 (1) (2002) F52–F59.
[58] I. Sipos, L. Tretter, V. Adam-Vizi, Quantitative relationship between inhibition of respiratory complexes and formation of reactive oxygen species in isolated nerve terminals, J. Neurochem. 84 (1) (2003) 112–118.
[59] A. Kulak, M. Cuenod, K.Q. Do, Behavioral phenotyping of glutathione-deficient mice: relevance to schizophrenia and bipolar disorder, Behav. Brain Res. 226 (2) (2012) 563–570.
[60] M. Boskovic, T. Vovk, B. Kores Plesnicar, I. Grabnar, Oxidative stress in schizophrenia, Curr. Neuropharmacol. 9 (2) (2011) 301–312.
[61] M. Kumar, R. Sandhir, Neuroprotective effect of hydrogen sulfide in hyperhomocysteinemia is mediated through antioxidant action involving Nrf2, NeuroMolecular Med. 20 (4) (2018) 475–490.
[62] M. Kumar, R. Sandhir, Hydrogen sulfide attenuates hyperhomocysteinemia-induced mitochondrial dysfunctions in brain, Mitochondrion 50 (2020) 158–169.
[63] J. Folbergrova, P. Jesina, Z. Drahota, V. Lisy, R. Haugvicova, A. Vojtiskova, J. Houstek, Mitochondrial complex I inhibition in cerebral cortex of immature rats following homocysteic acid-induced seizures, Exp. Neurol. 204 (2) (2007) 597–609.

[64] J.W. Muntjewerff, R.S. Kahn, H.J. Blom, M. den Heijer, Homocysteine, methylenetetrahydrofolate reductase and risk of schizophrenia: a meta-analysis, Mol. Psychiatr. 11 (2) (2006) 143–149.
[65] A. Nishi, S. Numata, A. Tajima, M. Kinoshita, K. Kikuchi, S. Shimodera, M. Tomotake, K. Ohi, R. Hashimoto, I. Imoto, M. Takeda, T. Ohmori, Meta-analyses of blood homocysteine levels for gender and genetic association studies of the MTHFR C677T polymorphism in schizophrenia, Schizophr. Bull. 40 (5) (2014) 1154–1163.
[66] A. Kale, N. Naphade, S. Sapkale, M. Kamaraju, A. Pillai, S. Joshi, S. Mahadik, Reduced folic acid, vitamin B12 and docosahexaenoic acid and increased homocysteine and cortisol in never-medicated schizophrenia patients: implications for altered one-carbon metabolism, Psychiatr. Res. 175 (1–2) (2010) 47–53.
[67] R. Ayesa-Arriola, R. Perez-Iglesias, J.M. Rodriguez-Sanchez, I. Mata, E. Gomez-Ruiz, M. Garcia-Unzueta, O. Martinez-Garcia, R. Tabares-Seisdedos, J.L. Vazquez-Barquero, B. Crespo-Facorro, Homocysteine and cognition in first-episode psychosis patients, Eur. Arch. Psychiatr. Clin. Neurosci. 262 (7) (2012) 557–564.
[68] B. Garcia-Bueno, M. Bioque, K.S. Mac-Dowell, M.F. Barcones, M. Martinez-Cengotitabengoa, L. Pina-Camacho, R. Rodriguez-Jimenez, P.A. Saiz, C. Castro, A. Lafuente, J. Santabarbara, A. Gonzalez-Pinto, M. Parellada, G. Rubio, M. P. Garcia-Portilla, J.A. Mico, M. Bernardo, J.C. Leza, Pro-/anti-inflammatory dysregulation in patients with first episode of psychosis: toward an integrative inflammatory hypothesis of schizophrenia, Schizophr. Bull. 40 (2) (2014) 376–387.
[69] E. Eren, A. Yegin, N. Yilmaz, H. Herken, Serum total homocystein, folate and vitamin B12 levels and their correlation with antipsychotic drug doses in adult male patients with chronic schizophrenia, Clin. Lab. 56 (11–12) (2010) 513–518.
[70] D.C. Goff, T. Bottiglieri, E. Arning, V. Shih, O. Freudenreich, A.E. Evins, D. C. Henderson, L. Baer, J. Coyle, Folate, homocysteine, and negative symptoms in schizophrenia, Am. J. Psychiatr. 161 (9) (2004) 1705–1708.
[71] N. Bouaziz, I. Ayedi, O. Sidhom, A. Kallel, R. Rafrafi, R. Jomaa, W. Melki, M. Feki, N. Kaabechi, Z. El Hechmi, Plasma homocysteine in schizophrenia: determinants and clinical correlations in Tunisian patients free from antipsychotics, Psychiatr. Res. 179 (1) (2010) 24–29.
[72] B. Misiak, D. Frydecka, R. Slezak, P. Piotrowski, A. Kiejna, Elevated homocysteine level in first-episode schizophrenia patients–the relevance of family history of schizophrenia and lifetime diagnosis of cannabis abuse, Metab. Brain Dis. 29 (3) (2014) 661–670.
[73] N.D. Petronijevic, N.V. Radonjic, M.D. Ivkovic, D. Marinkovic, V.D. Piperski, B. M. Duricic, V.R. Paunovic, Plasma homocysteine levels in young male patients in the exacerbation and remission phase of schizophrenia, Progress in neuro-psychopharmacology & biological psychiatry 32 (8) (2008) 1921–1926.
[74] H.G. Dunn, T.L. Perry, C.L. Dolman, Homocystinuria. A recently discovered cause of mental defect and cerebrovascular thrombosis, Neurology 16 (4) (1966) 407–420.
[75] N.A. Carson, D.C. Cusworth, C.E. Dent, C.M. Field, D.W. Neill, R.G. Westall, Homocystinuria: a new inborn error of metabolism associated with mental deficiency, Arch. Dis. Child. 38 (201) (1963) 425–436.
[76] R.N. Schimke, V.A. McKusick, T. Huang, A.D. Pollack, Homocystinuria. Studies of 20 families with 38 affected members, J. Am. Med. Assoc. 193 (1965) 711–719.
[77] H.H. White, L.P. Rowland, S. Araki, H.L. Thompson, D. Cowen, Homocystinuria, Arch Neurol 13 (5) (1965) 455–470.
[78] N.C. Allen, S. Bagade, M.B. McQueen, J.P. Ioannidis, F.K. Kavvoura, M.J. Khoury, R.E. Tanzi, L. Bertram, Systematic meta-analyses and field synopsis of genetic association studies in schizophrenia: the SzGene database, Nat. Genet. 40 (7) (2008) 827–834.
[79] T. Ohnishi, S. Balan, M. Toyoshima, M. Maekawa, H. Ohba, A. Watanabe, Y. Iwayama, Y. Fujita, Y. Tan, Y. Hisano, C. Shimamoto-Mitsuyama, Y. Nozaki, K. Esaki, A. Nagaoka, J. Matsumoto, M. Hino, N. Mataga, A. Hayashi-Takagi, K. Hashimoto, Y. Kunii, A. Kakita, H. Yabe, T. Yoshikawa, Investigation of betaine as a novel psychotherapeutic for schizophrenia, EBioMedicine 45 (2019) 432–446.
[80] M. Hussain, K. Bork, V.S. Gnanapragassam, D. Bennmann, K. Jacobs, A. Navarette-Santos, B. Hofmann, A. Simm, K. Danker, R. Horstkorte, Novel insights in the dysfunction of human blood-brain barrier after glycation, Mech. Ageing Dev. 155 (2016) 48–54.
[81] B. Wang, T.Y. Aw, K.Y. Stokes, The protection conferred against ischemia-reperfusion injury in the diabetic brain by N-acetylcysteine is associated with decreased dicarbonyl stress, Free Radic. Biol. Med. 96 (2016) 89–98.
[82] G.M. Khandaker, L. Cousins, J. Deakin, B.R. Lennox, R. Yolken, P.B. Jones, Inflammation and immunity in schizophrenia: implications for pathophysiology and treatment, Lancet Psychiatry 2 (3) (2015) 258–270.
[83] N. Muller, Inflammation in schizophrenia: pathogenetic aspects and therapeutic considerations, Schizophr. Bull. 44 (5) (2018) 973–982.
[84] J.C. Tobon-Velasco, E. Cuevas, M.A. Torres-Ramos, Receptor for AGEs (RAGE) as mediator of NF-kB pathway activation in neuroinflammation and oxidative stress, CNS Neurol. Disord. - Drug Targets 13 (9) (2014) 1615–1626.
[85] K. Toriumi, M. Miyashita, K. Suzuki, N. Yamasaki, M. Yasumura, Y. Horiuchi, A. Yoshikawa, M. Asakura, N. Usui, M. Itokawa, M. Arai, Vitamin B6 deficiency hyperactivates the noradrenergic system, leading to social deficits and cognitive impairment, Transl. Psychiatry 11 (1) (2021) 262.
[86] S. Anders, A. Reyes, W. Huber, Detecting differential usage of exons from RNA-seq data, Genome Res. 22 (10) (2012) 2008–2017.